Phosphorylation of the Ribosomal Protein RPL12/uL11 Affects Translation during Mitosis

Imami K., Milek M., Bogdanow B., Yasuda T., Kastelic N., Zauber H., Ishihama Y., Landthaler M., Selbach M.

This is the final version of the accepted manuscript. The original article has been published in final edited form in:

Molecular Cell
2018 OCT 04 ; 72(1): 84-98
2018 SEP 13 (first published online: final publication)
doi: 10.1016/j.molcel.2018.08.019

Publisher: Cell Press / Elsevier

Phosphorylation of the ribosomal protein RPL12/uL11 affects translation during mitosis

Koshi Imami[1, 4*], Miha Milek[1], Boris Bogdanow[1], Tomoharu Yasuda[1, 5], Nicolai Kastelic[1], Henrik Zauber[1], Yasushi Ishihama[4], Markus Landthaler[1, 2], Matthias Selbach[1,3, 6 *]

[1] Max Delbrück Center for Molecular Medicine, Robert-Rössle-Str. 10, D-13092 Berlin, Germany

[2] IRI Life Sciences, Institute für Biologie, Humboldt Universität zu Berlin, Philippstraße 13, 10115 Berlin

[3] Charité-Universitätsmedizin Berlin, 10117 Berlin, Germany

[4] Present address: Department of Molecular and Cellular BioAnalysis, Kyoto University, 606-8501, Kyoto, Japan

[5] Present address: Department of Molecular and Cellular Biology, Kyushu University, 812-8582, Fukuoka, Japan

[6] Lead contact

* Corresponding authors:

Matthias Selbach (lead corresponding author)
Max Delbrück Centrum for Molecular Medicine
Robert-Rössle-Str. 10, D-13092 Berlin, Germany
Tel.: +49 30 9406 3574
Fax.: +49 30 9406 2394
email: matthias.selbach@mdc-berlin.de

Koshi Imami
Department of Molecular and Cellular BioAnalysis
Kyoto University
606-851, Kyoto, Japan
email: imami.koshi.3z@kyoto-u.ac.jp

Summary

Emerging evidence indicates that heterogeneity in ribosome composition can give rise to specialized functions. Until now, research mainly focused on differences in core ribosomal proteins and associated factors. The impact of posttranslational modifications has not been studied systematically. Analyzing ribosome heterogeneity is challenging since individual proteins can be part of different subcomplexes (40S, 60S, 80S and polysomes). Here, we develop polysome proteome profiling to obtain unbiased proteomic maps across ribosomal subcomplexes. Our method combines extensive fractionation by sucrose gradient centrifugation with quantitative mass spectrometry. The high resolution of the profiles allows us to assign proteins to specific subcomplexes. Phosphoproteomics on the fractions reveals that phosphorylation of serine 38 in RPL12/uL11, a known mitotic CDK1 substrate, is strongly depleted in polysomes. Follow-up experiments confirm that RPL12/uL11 phosphorylation regulates translation of specific subsets of mRNAs during mitosis. Together, our results show that posttranslational modification of ribosomal proteins can regulate translation.

Introduction

The ribosome is a large ribonucleoprotein complex which translates mRNAs into proteins and thus plays a central role in all living cells (Bashan and Yonath, 2008; Schmeing and Ramakrishnan, 2009; Steitz, 2008). The translation efficiency of mRNAs is a key mediator of protein abundance and thus gene expression control (Schwanhäusser et al., 2011). It is now clear that regulatory elements of mRNAs can modulate every step of protein synthesis from initiation to termination (Truitt and Ruggero, 2017). These cis-regulatory elements mediate the dynamic interaction of mRNAs with trans-acting factors such as RNA-binding proteins or microRNAs (Carpenter et al., 2014). Also, mRNAs can be modified to recruit or repel specific binders (Edupuganti et al., 2017; Wang et al., 2015).

Ribosomes themselves are traditionally seen as homogenous molecular machines with little regulatory potential. However, the ribosome filter hypothesis proposes that ribosomal subunits act themselves as regulatory elements (or "filters") that mediate interactions with particular mRNAs and control their translation (Mauro and Edelman, 2002). Emerging evidence suggests that different types of ribosomes exist: Heterogeneity can occur at the level of (i) rRNAs, (ii) core ribosomal proteins (RPs), (iii) ribosome-associated proteins and (iv) post-translational modifications (PTMs) (reviewed in (Mauro and Matsuda, 2016; Shi and Barna, 2015)). Recent examples include the core RPs RPL38/eL38 (Xue et al., 2014), RPL40/eL40 (Lee et al., 2013), RPL10A/uL1 and RPS25/eS25 (Shi et al., 2017). These RPs appear to selectively regulate translation of distinct subpools of mRNAs (Shi et al., 2017; Xue et al., 2014). Also, LIN28A (Cho et al., 2012) and PKM2 (Simsek et al., 2017) are ribosome-associated proteins localized at the endoplasmic reticulum (ER) and confer specialized functions to ribosomes translating proteins into the ER. Many aspects of ribosome heterogeneity remain poorly understood. In particular, the role of PTMs for ribosome function is unclear: While proteomics identified many modification sites in RPs (Wilhelm et al., 2014), only few of these modifications have been reported to be involved in translational control (Gressner and Wool, 1974; Martin et al., 2014; Spence et al., 2000). No systematic analysis on the impact of ribosomal PTMs on protein translation has so far been reported.

Mass spectrometry (MS)-based quantitative proteomics (Aebersold and Mann, 2016) is a powerful technology to systematically study ribosome composition. For example, the Williamson lab used quantitative proteomics to study ribosome assembly in *E. coli (Chen and Williamson, 2013; Davis et al., 2016)*. Proteomic analyses in mammals identified more than 1,500 proteins

as the so-called “mammalian riboproteome" (Aviner et al., 2017; Reschke et al., 2013). Recently, tagged endogenous RPs were pulled down to identify associated proteins (Simsek et al., 2017). These experiments yielded exciting insights. However, it is important to note that the same RP is part of several, functionally different ribosome subcomplexes: the small and large subunits (that is, 40S and 60S), monosomes (80S) and polysomes. In addition, the small subunit also forms 43S and 48S subcomplexes during translation initiation (Sonenberg and Hinnebusch, 2009). Affinity purification with tagged RPs cannot distinguish between these subcomplexes. Ribosome heterogeneity across different subcomplexes has not yet been analyzed systematically.

Here, we developed polysome proteome profiling (3P) -- a method that combines extensive sucrose gradient fractionation with accurate quantification -- to systematically characterize ribosome composition across subcomplexes. Using this method we obtain proteomic maps of translating ribosomes at high resolution. These data allows us to assess the distribution of core RPs and ribosome-associated proteins across subcomplexes. Quantitative phosphoproteomics in 3P fractions reveals differences in the phosphorylation state of RPs between subcomplexes. Intriguingly, follow-up experiments reveal that phosphorylation of RPL12/uL11 on serine 38 affects mitotic translation.

Results

Polysome proteome profiling yields high resolution proteomic maps of translating ribosomes

The gold standard method to resolve different ribosome subcomplexes is sucrose density centrifugation (Britten and Roberts, 1960). However, cytosolic fractions generated by this method contain many other proteins in addition to ribosomes. Distinguishing specific ribosome components from contaminants is a major challenge. Several proteomic techniques use co-migration to study protein complexes (Kristensen and Foster, 2013). The principle of these methods is that lysates are separated into fractions under native conditions (Havugimana et al., 2012; Heide et al., 2012; Kristensen et al., 2012). Quantitative shotgun proteomics then reveals which proteins co-fractionate and are thus part of the same complex. We reasoned that combining sucrose density gradient centrifugation and quantitative proteomics should yield high resolution maps of cytosolic ribosomes. We refer to this approach as "polysome proteome profiling" (3P). It consists of three steps: First, sucrose gradient centrifugation is used to obtain many density fractions covering the 40S, 60S and 80S complexes as well as polysomes. Second, the protein abundance in all fractions is accurately quantified relative to an internal reference standard. Third, the quantitative profiles obtained in this manner are compared to ribosome consensus profiles to identify which proteins are indeed ribosome-associated.

The quality of data obtained depends on the number of fractions and the accuracy of quantification. We therefore sampled many fractions along the sucrose gradient and used stable isotope labeling by amino acids in cell culture (SILAC) for quantification (Ong et al., 2002) (Figure 1A): First, lysates from differentially SILAC labeled cells were individually resolved into 36 fractions. Next, individual fractions from light and heavy cells were combined as biological duplicates. As an internal standard, all fractions from medium-heavy cells were first pooled and then spiked into each fraction from the combined light and heavy mixtures. Hence, the ratios of light and heavy peptide peaks relative to the medium-heavy internal standard directly reflect protein abundance across the sucrose gradient (Figure 1B). Key advantages of this setup are the use of an internal standard and the high number of fractions, which yields accurate high resolution profiles.

We analyzed two independent biological replicates of two HEK293 and HeLa cells and identified 4,030 proteins in total (Table S1). This list contains all known RPs except for RPL41/eL41 and RS4Y1/RS4Y2/eS4. RPL41/eL41 has no tryptic peptides of sufficient length and

RS4Y1/RS4Y2/eS4 is male-specific and thus not expressed in the two female cell lines used. To ensure accurate quantification, we required proteins to be quantified in at least ten fractions, which reduced the number of proteins to 1,609. Clustering of ratios revealed high reproducibility between biological replicates and cell lines (Figure 1C). Intriguingly, all proteins of the small (40S, n=32) and large (60S, n=44) subunit of the ribosome fell into two distinct clusters (Figure 1B). Hence, if these proteins were not yet known to be ribosomal proteins, our analysis would have identified them and assigned them to the correct subunit. Mitochondrial RPs clustered separately, even though the large subunit of the mitochondrial ribosome and the small subunit of the cytosolic ribosome have very similar sedimentation rates (39S and 40S, respectively). Plotting the profiles of all RPs revealed separate peaks for the 40S, 60S and 80S complexes that correlated well with RNA profiles obtained from the same samples (Figure 1D). Polysomes with two, three, four and more ribosomes per mRNA were also clearly distinguishable. Hence, our proteomic profiles are indeed of high resolution and can differentiate between ribosomal states.

Composition of the core ribosome

Core RPs are traditionally thought to have a fixed stoichiometry across different states. A recent paper challenged this view and reported that in mouse ES and yeast cells, some RPs appear to be more abundant in monosomes than in polysomes and *vice versa* (Slavov et al., 2015). However, this study used only five fractions and lacked an internal standard, limiting its resolution and accuracy. In our data, all 76 quantified RPs showed similar abundance profiles across monosome and polysome fractions in both HEK293 and HeLa cells. Polysome proteome profiles from mouse ES cells confirmed this finding (Figure S1A and B). We conclude that, in contrast to the previous report, the composition of the core ribosome does not significantly differ between monosomes and polysomes in these cell lines. Importantly, this finding does not exclude that ribosomes with different core RP composition can exist (Ferretti et al., 2017; Shi et al., 2017).

Ribosome-associated proteins

A study identified ~1.500 proteins in polysome fractions from prostate cancer cells lines as the so-called “mammalian riboproteome” (Reschke et al., 2013). We identified 2,327 proteins in

polysome fractions of HEK293 and HeLa cells, including many of the previously published ones (Figure 2A, upper panel). However, since polysome fractions are crude, not all proteins in these lists are ribosome-associated. For example, both our and the published data are enriched in mitochondrial RPs (Figure 2A, lower panel). Hence, the so-called "mammalian riboproteome" (Reschke et al., 2013) is contaminated by proteins derived from co-sedimenting complexes.

True polysome-associated proteins should follow the abundance profile of RPs. Therefore, we compared the profiles of candidate proteins to a polysome consensus profile obtained by averaging over all RPs (Figure S2A) and computed the mean squared deviation ("MSD values") between a given profile and the consensus (Figure 2B) (Andersen et al., 2003; Foster et al., 2006). MSD values were reproducible between biological duplicates and cell lines (Figure 2C inset, Figure S2B). We then used a MSD cut-off to define polysome-associated proteins and only kept proteins identified in both biological replicates (Table S1). This eliminated all contaminating mitochondrial RPs (Figure 2D). To benchmark our method we created a reference set using GO terms, the STRING database (Szklarczyk et al., 2017) and RNAi screening data (Badertscher et al., 2015; Wild et al., 2010) (see Methods and Table S2 for the reference set). We found that our data captures known ribosome-related proteins with very good sensitivity and specificity (Figure 2E).

We identified 145 polysome-associated proteins (Figures 2F and S3, Table S1 "category 1"). Over 70% of these proteins are ribosome-related and/or RNA-binding (Figures 2F and 2G). Estimating absolute protein abundance via intensity-based absolute quantification (iBAQ) (Schwanhäusser et al., 2011) revealed that polysome-associated proteins were 1-5 orders of magnitude less abundant than core RPs, suggesting that they associate with only a subset of ribosomes (Figure 2H). We captured several known polysome interacting proteins (Figures 2I) such as RACK1 (Thompson et al., 2016), STAU1 (Ricci et al., 2014) and SEC61 (Voorhees et al., 2014). The data reveals ribosome association with subunit resolution: For example, RACK1 and STAU1 have been reported to interact with the 40S and 60S subunits, respectively (Ricci et al., 2014; Sengupta et al., 2004), which is reflected in the profiles (Figure 2I). Also, the polyA binding protein PABPC4 associated with 80S and polysomes but not with individual subunits. Computing MSD values using either 40S or 60S RPs as reference (Figure S2A) allowed us to categorize ~46% of our 145 polysome associated proteins as 40S or 60S specific interactors (Figures 2J and S2C).

84 of the 145 polysome interactors have not been described previously. This includes kinases, deubiquitinating enzymes and other interesting proteins, highlighting the diversity of ribosome

function. We provide individual profiles for all 145 proteins (class I category) and corresponding MSD value plots as a supplementary dataset ("polysome_associated_proteins.pdf"). In addition, we provide profiles for 40 proteins that passed the cut-offs in only one of the two replicates in either cell line (Table S1 "category 2"), including known proteins like LARP4 and UPF1. 4 out of 5 tested new candidates could be validated (Figure S2D and E).

Phosphorylation of RPs

Many RPs carry posttranslational modifications (PTMs), but their function is largely enigmatic (Simsek and Barna, 2017). For example, while phosphorylation of RPS6/eS6 was identified over 40 years ago (Gressner and Wool, 1974), its functional relevance is still unclear (Meyuhas, 2015). We reasoned that combining 3P and phosphoproteomics might identify sites with regulatory potential. To this end, we used TiO_2-based enrichment (Rappsilber et al., 2007) on our fractions (Figure 1A). We identified 1,819 class 1 phosphorylation sites (Olsen et al., 2006) in 1,143 proteins, including 46 phosphosites in RPs (Figure 3A). To identify sites that might regulate ribosome function we compared profiles of all phosphopeptides with the consensus profiles (Figure 3B). Most phosphopeptide profiles resembled the consensus profiles, including the key phosphorylation sites in RPS6/eS6 (Figure 3C). This is interesting since S6 phosphorylation was originally thought to regulate translation. Our data corroborates genetic studies showing that S6 phosphorylation is dispensable for polysome association (Ruvinsky et al., 2005).

Of all phosphosites covered, pS38 in RPL12/uL11 deviated most from the consensus profile (Figure 3B and 3D): pS38 levels were high in 60S and 80S fractions but low in polysome fractions. To validate this finding, we generated stable HEK293 cell lines expressing FLAG/HA-tagged wild-type (WT) RPL12/uL11, a phosphomimetic S38D mutant or a non-phosphorylatable S38A mutant. Sucrose gradient fractionation showed that tagged WT RPL12/uL11 is incorporated into ribosomes and behaves similarly to the endogenous protein (Figure 3E, see Figure S3A for different clones). The S38D mutant was strongly depleted in polysomes, corroborating the proteomic data. Of note, the mutant was incorporated into ribosomes, suggesting that dephosphorylation is not needed for ribosome assembly. The S38A mutant behaved similarly to the wild-type, indicating that RPL12/uL11 phosphorylation is not required for ribosome assembly nor translation initiation. We conclude RPL12/uL11 S38 phosphorylation is depleted in polysomes and might thus regulate translation.

RPL12/uL11 S38 is an evolutionarily conserved mitotic CDK1 substrate

The sequence surrounding S38 is highly conserved in eukaryotes and matches a consensus motif for CDK1 substrates (pS-P-K-K) (Figure 4A). Phosphorylation of RPL12/uL11 on S38 has been observed in several species (Gnad et al., 2011). Phosphoproteomic data across the cell cycle in HeLa cells revealed that RPL12/uL11 S38 phosphorylation peaks in mitosis and reaches the lowest level in S phase (Figure 4B) (Dephoure et al., 2008; Olsen et al., 2010). Consistently, CDK1/2 phosphorylates RPL12/uL11 *in vitro (Chi et al., 2008)*. Also, the CDK1-cyclin B complex physically associates with RPL12/uL11 during mitosis in HeLa cells (Pagliuca et al., 2011). Finally, experiments with an analog sensitive CDK1 variants indicate that CDK1 directly phosphorylates RPL12/uL11 on S38 during mitosis in yeast (Holt et al., 2009). Thus, RPL12/uL11 S38 is an evolutionarily conserved mitotic CDK1 substrate. Similar to other CDK1 substrates, the occupancy of S38 phosphorylation in mitosis is as high as ~70% (Olsen et al., 2010).

RPL12/uL11 S38 phosphorylation does not globally affect translation

RPL12/uL11 is located close to the A-site in the P stalk of the ribosome -- a site where multiple ribosomal GTPases such as an elongation factor eEF1A and a termination factor eRF1 bind (Liu et al., 2015; Spahn et al., 2004; Taylor et al., 2012) (Figure 3A). Since knockdown of RPL12/uL11 attenuates translation elongation in human and yeast cells (Briones et al., 1998; Veit et al., 2016) we hypothesized that phosphorylation might globally affect translation during mitosis. Early experiments suggested that translation is globally suppressed in mitosis (Fan and Penman, 1970; Wilker et al., 2007). However, this suppression might be an artifact caused by the drugs employed (Coldwell et al., 2013; Shuda et al., 2015). To measure protein synthesis without drug treatment we used metabolic pulse labeling in a flow cytometric assay (Kiick et al., 2001; Shuda et al., 2015) (Figure 4C). HEK293 cells transiently expressing FLAG/HA tagged RPL12/uL11 WT, S38D or S38A were pulse-labeled with azidohomoalanine (AHA) to measure global protein synthesis (Figure 4D left panel). Histone H3 pS10 was used as a mitotic marker (Figure 4C). We found no significant difference in global protein synthesis between the RPL12/uL11 variants -- neither in interphase nor in mitosis (Figure 4D right panel). All we observed was a slight reduction in the fraction of mitotic cells in both mutants (Figure 4E). We conclude that RPL12 phosphorylation does not have a major impact on global protein synthesis.

RPL12/uL11 S38 phosphorylation regulates translation of mitosis-related mRNAs

We next asked whether RPL12/uL11 phosphorylation might regulate translation of specific subsets of mRNAs. To quantify differences in protein production between the D and the A mutant we used pSILAC (Schwanhäusser et al., 2009) (Figure 5A left panel; Table S3). We then selected a subset of proteins that had been reported to be preferentially translated in mitosis according to ribosome profiling data (Stumpf et al., 2013). Translation of this subset was significantly higher in cells with S38D ribosomes, consistent with our hypothesis (Figure 5A, right). Conversely, S38A cells preferentially translated mRNAs that are more actively translated in S phase. Hence, phosphorylation of S38 appears to regulate translation of specific mRNAs.

Interpretation of the pSILAC data is complicated by the fact the cells express both tagged and endogenous (that is, wild-type) RPL12/uL11. We next sought to analyze only ribosomes containing the tagged variants (Figure 5B, left panel). We isolated monosomes by sucrose gradient centrifugation from HEK293 cells expressing tagged RPL12/uL11 WT, S38D or S38A. These monosome fractions contain both ribosomes with endogenous RPL12/uL11 and with tagged RPL12/uL11 variants. We then used an anti-FLAG antibody to immunoprecipitate ribosomes with tagged RPL12/uL11 from monosome fractions (Figure S3B). Both the precipitated ribosomes and the corresponding monosome fractions were analyzed by RNA-seq. Hence, every immunoprecipitated sample is accompanied by its own internal control (i.e. the corresponding whole monosome fraction). We classified mRNAs according to their enrichment ratios (IP vs monosome fraction) for different combinations of RPL12/uL11 variants (Figure S3C; Table S4). The differences in mRNAs enrichment between S38D and S38A were small. However, several well-known mitotic factors such as cohesins (SMC3, SMC1B), mitotic spindle proteins (DLGAP5, KIF11, TPX2), kinetochore components (CENP-C) and mitotic cyclins B1 and B2 (CCNB1, CCNB2) were in the high enrichment group (log2 D/A, Table S4). Gene ontology analysis of transcripts associated with the phosphomimetic mutant revealed enrichment of terms related to the cell cycle ("cell cycle", "regulation of cell cycle") and posttranscriptional regulation ("translation", "RNA processing", "ribosomal large subunit biogenesis") (Fig. 5 C).

To globally assess mitosis-specific translation, we calculated the ratios of ribosome protected fragments during mitosis and S phase in ribosome profiling data (Stumpf et al., 2013) for the different subgroups. We found that monosomes containing S38D preferentially associated with

mRNAs with higher mitosis-specific ribosome occupancy than monosomes with S38A (Figure 5B, right panel). Comparing S38D to wild-type RPL12/uL11 revealed the same trend (Figure S3D upper panel). In contrast, S38A ribosomes and wild-type monosomes did not show significant differences (Figure S3D bottom panel). This validates the pSILAC data and confirms the hypothesis that RPL12/uL11 phosphorylation shifts the ribosomal translation profile towards mitosis.

We next wanted to identify mRNA sequence features correlated to preferential binding to the D or A mutant. Genes in the category “M phase of the mitotic cell cycle” have been reported to display a characteristic codon usage pattern, typically with A or U in the last codon (that is, “wobble”) position (Gingold et al., 2014). Therefore, we followed a strategy similar to (Presnyak et al., 2015) to assess if codon frequencies correlate with observed differences in enrichment values between the D and the A mutant. Strikingly, the 10 codons with the strongest positive and negative correlation all showed a A/U or G/C at the third position, respectively (Fig. 5D). Hence, mRNAs associated with the phosphomimetic mutant and mRNAs encoding proteins with a function in mitosis show the same A/U preference in the wobble position. The same trend is also seen in the total AU content (Fig. 5E).

In addition to translation itself, protein production can be affected by changes in mRNA levels. While mitotic chromatin was previously thought to be transcriptionally silent, a recent study found that many mRNAs are synthesized during mitosis (Palozola et al., 2017). Integrating these data with ours revealed that mitotically transcribed mRNAs preferentially associate with ribosomes carrying the D mutant, providing another link between RPL12/uL11 phosphorylation and mitosis (Fig. 5F). When we only consider mRNAs that are strongly transcriptionally induced during mitosis, the difference between the D and A mutant is less pronounced. It thus appears that protein production in mitosis is controlled by at least two mechanisms acting on different sets of genes: One is up-regulated transcriptionally while the other is continuously transcribed and regulated via RPL12/uL11 phosphorylation at the level of the ribosome. The mRNAs in these two subsets can be distinguished by their G/C content, consistent with the observed codon bias (Fig. 5G).

Translational regulation through RPL12/uL11 phosphorylation is conserved in mouse B cells

To further validate our findings we used CRISPR to mutate the endogenous RPL12/uL11 gene in mouse B lymphoma cells (19DN) (Sander et al., 2015). We obtained both a homozygous RPL12/uL11 S38D and a S38A cell line (Figure S4A and B). Repeating the above-mentioned experiments with these cells confirmed the key findings from HEK293 cells: First, wild-type, S38D and S38A mutant cells synthesize similar amounts of protein (Figure 6A left panel). Second, we observed a slight reduction in the fraction of mitotic cells in both mutants (Figure 6A right panel). Third, the S38D mutant preferentially translates mitosis-related transcripts (Figure 6B and Figure S5A). To validated these we randomly selected 50 proteins with absolute log2 FCs > 0.1 in the pSILAC data and designed parallel reaction monitoring (PRM) assays for them using Picky (Zauber et al., 2018) (see Methods). This confirmed differential regulation for 34 of the 41 identified proteins (Figure S5B). These data indicate that the regulatory function of RPL12/uL11 phosphorylation is conserved and partially cell type independent.

Having a model system in which the entire pool of endogenous RPL12/uL11 is replaced by the phosphomimetic or non-phosphorylatable mutant allows us to use ribosome profiling as an additional read-out for translation (Ingolia, 2016). We performed ribosome profiling in S38D and S38A B cells. Ribosome protected fragment (RPFs) showed the characteristic periodicity that indicates genuine translation (Figure S5C-E). Proteins that are differentially translated according to our pSILAC data also showed highly significant differences in RPFs between the D and the A mutant in the ribosome profiling data (Fig. 6C and Figure S5F). Hence, two independent read-outs provide consistent results. To define our own subset of mitotically translated mRNAs we also performed ribosome profiling on mitotic wild-type cells (Figure S5G, S5H). Comparing RPFs in mitotic and asynchronous wild-type cells allowed us to define a set of 692 mRNAs that are preferentially translated in mitosis and 792 mRNAs which are more translated in asynchronous cells. The mitotic subset is functionally linked to translation and RNA processing (Figure S5I), consistent with a previous report in human cells (Park et al., 2016). We then compared the translation of these subsets in the D and the A mutant. Again, we observed that cells expressing phosphomimetic RPL12/uL11 exhibited higher RPFs for the mitotic subset than cells expressing the non-phosphorylatable mutant (Figure 6D and Table S6). Altogether, results from three independent experimental approaches (pSILAC, RNA-seq of affinity purified monosomes, ribosome profiling) and two different model systems (human HEK cells, mouse B cells) consistently indicate that RPL12/uL11 pS38 phosphorylation influences mitotic translation.

Discussion

The polysome proteome profiling (3P) approach presented here provides proteomic maps of translating ribosomes. The high resolution of these maps allows us to unambiguously assess the composition of different subcomplexes -- a key advantage over conventional affinity purification approaches (Simsek et al., 2017). The method does not involve tagging or overexpression and can thus be readily applied to different tissues or model organisms. Despite these advantages, it is also important to keep the limitations of the method in mind. First, high resolution profiles requires analysis of many fractions and thus long measurement times. Second, 3P (and classical affinity purification) involves cell lysis, which might result in loss of weak interactions or artifactual binding in lysates. Third, since individual fractions contain thousands of ribosomes, the data represents the average for many complexes in every density range. For example, while ribosomes with different core RP composition have been reported to exist (Ferretti et al., 2017; Shi et al., 2017), this heterogeneity at the level of single ribosomes cannot be resolved by 3P. In fact, our absolute abundance estimates indicate that several core RPs are sub-stoichiometric, supporting the view that the composition of individual ribosomes can indeed differ (Figure 2H).

Our data indicates that the core RP composition does not significantly differ between monosomes and polysomes (Figure 1D), in contrast to a previous report (Slavov et al., 2015). Also, while a previous study reported over 1,000 ribosome-associated proteins (Reschke et al., 2013), our rigorous profiling indicates that most of them are contaminants (Figures 2A and 2D). We identify a high confidence set of 145 polysome associated proteins with a wide range of biological functions (Figure 2F). Finally, our phosphoproteomic analysis identifies S38 in RPL12/uL11 as phosphorylation site that regulates translation during mitosis.

Translation is traditionally thought to be globally suppressed during mitosis (Fan and Penman, 1970), but more recent data challenges this view (Aviner et al., 2013; Park et al., 2016; Stumpf et al., 2013; Tanenbaum et al., 2015). Several cis-regulatory elements in mRNAs such as internal ribosome entry sites (IRESs), 5' terminal oligopyrimidine tracts (TOPs), 5’ caps and poly(A) tail length have been reported to control mitotic translation (Park et al., 2016; Shuda et al., 2015; Wilker et al., 2007). Splicing factors bind polysomes in mitosis and affect translation of specific messages (Aviner et al., 2017). Modifications of the ribosome itself has not yet been reported to regulate translation in a cell cycle dependent-manner. We studied the impact of

RPL12/uL11 phosphorylation on translation using phosphomimetic and non-phosphorylatable mutants. Based on these experiments we arrived at three conclusions. First, phosphorylation does not have a major impact on total protein synthesis (Figure 4). Second, RPL12/uL11 phosphorylation shifts protein production of ribosomes towards a more mitotic translation profile (Figure 5A). Third, ribosomes with phosphorylated RPL12/uL11 associate with mRNAs that are more actively translated during mitosis (Figure 5B). An important caveat in these experiments is that the phosphomimetic (or non-phosphorylatable) mutant may behave differently than endogenous phosphorylated (or non-phosphorylated) RPL12/uL11. However, we observed that the sucrose gradient profiles of the mutants resembled the profiles of phosphorylated and non-phosphorylated RPL12/uL11 (Figures 3E and S4A). Thus, the mutants appear to reflect key aspects of RPL12/uL11 phosphorylation.

It is remarkable that HEK 293 cells overexpressing phosphomimetic and non-phosphorylatable RPL12/uL11 variants and the corresponding mutant B cell lines do not show more dramatic phenotypes. This might be due to three (not mutually exclusive) reasons. First, the observed differences between the variants are quite small, suggesting that phosphorylation modulates rather than switches ribosome function. Second, the eukaryotic cell cycle is robustly designed and comprises multiple redundant components and feedbacks (Li et al., 2004; Zhu and Mao, 2015). Therefore, cell perturbations can be tolerated, as for example seen in the remarkably subtle phenotypes of Cdk2 and cyclin E knock-out mice (Geng et al., 2003; Ortega et al., 2003). Third, loss of function mutations in individual RP coding genes often have cell type specific and sometimes subtle phenotypes (Mauro and Matsuda, 2016; Shi and Barna, 2015). Interestingly, the profile of the S38D RPL12/uL11 in B cells follows the 60S consensus profile without depletion in polysomes (Figure S4C and D). Whether this reflects compensatory mechanisms is not clear. More generally, the relationship between polysome depletion of phosphorylated RPL12/uL11 and mitotic translation remains to be investigated. While actively translated mRNAs are believed to be limited to polysomes, a recent study showed that also monosomes contribute to translation of mRNAs such as short open reading frames (ORFs) and long ORFs with slow initiation rates that encode regulatory proteins (Heyer and Moore, 2016). In this context, it is important to note that ribosomes with phosphomimetic and non-phosphorylatable RPL12/uL11 interact with different mRNAs even when both are purified from monosome fractions (Figure 5B). Thus, selective mRNA binding is already seen in monosomes and does not require polysome formation.

How does RPL12/uL11 phosphorylation regulate translation? RPL12/uL11 is located in the ribosomal GTPase associated center (GAC) to which translational GTPases access in order to stimulate their hydrolytic activity during protein synthesis. RPL12/uL11 regulates elongation through interaction with two elongation GTPases, eEF1A and eEF2 (Briones et al., 1998; Veit et al., 2016; Wawiórka et al., 2016), which drive aminoacyl-tRNA decoding and translocation of the new peptidyl-tRNA during elongation, respectively. The phosphorylation site is proximal to the binding site for eEF1A (Liu et al., 2015) and eEF2 (Anger et al., 2013). It is tempting to speculate that phosphorylated RPL12/uL11 modulates binding affinity towards specific tRNAs, thereby facilitating elongation of specific mRNAs (Presnyak et al., 2015). In this context, the observed codon/GC content bias is noteworthy (Figure 5E). While the functional relevance of this observation is unclear, it is interesting that both mRNAs associated with the D mutant (Figure 5D) and mRNAs that are functionally related to mitosis (Gingold et al., 2014) are AU-rich. Since RPL12/uL11 depletion causes initiation delay, phosphorylation may alternatively/additionally regulate the initiation step (Wawiórka et al., 2016).

In summary, our proteomic picture of ribosome heterogeneity reveals that RPL12/uL11 phosphorylation regulates mitotic translation. This further supports the ribosome filter hypothesis (Mauro and Edelman, 2002) and extends the recent finding that heterogeneous ribosomes preferentially translate distinct subpools of mRNAs (Shi et al., 2017). To our knowledge, this is the first study demonstrating that posttranslational modifications of RPs can affect translation. Since many RPs can be modified by many types of PTMs, other examples may soon emerge.

Acknowledgements

We would like to thank Christian Sommer and Martha Hergeselle for excellent technical assistant, Katrina Meyer for editing the manuscript, Neelanjan Mukherjee for advice on RNA-seq analyses as well as Hans-Peter Rahn (all MDC) for helping FACS experiments. We also thank Nelleke Spruijt and Michiel Vermeulen (Radboud University) for kindly providing mouse ES cells.

Author contributions

K.I. and M.S. conceived and designed the study. K.I. performed most wet lab experiments and contributed to data analysis under the supervision of M.S. and Y.I.. M.M. generated the stable cell lines and performed the monosome-RNA-seq experiment. M.M and N.K. performed the

ribosome profiling experiment and analyzed the data under the supervision of M.L.. H.Z. performed PRM assay and analyzed the data. B.B. contributed to bioinformatic analyses including MSD calculation, protein complex enrichment and ROC analysis. T.Y. and K.I. performed the CRISPR and flow cytometry experiments. All authors interpreted data. M.S. supervised the project. K.I. and M.S. wrote the manuscript with input from all authors.

Declaration of interests

The authors declare no competing interests.

References

Aebersold, R., and Mann, M. (2016). Mass-spectrometric exploration of proteome structure and function. Nature *537*, 347–355.

Anders, S., Pyl, P.T., and Huber, W. (2014). HTSeq - A Python framework to work with high-throughput sequencing data.

Andersen, J.S., Wilkinson, C.J., Mayor, T., Mortensen, P., Nigg, E.A., and Mann, M. (2003). Proteomic characterization of the human centrosome by protein correlation profiling. Nature *426*, 570–574.

Anger, A.M., Armache, J.-P., Berninghausen, O., Habeck, M., Subklewe, M., Wilson, D.N., and Beckmann, R. (2013). Structures of the human and Drosophila 80S ribosome. Nature *497*, 80–85.

Aviner, R., Geiger, T., and Elroy-Stein, O. (2013). Novel proteomic approach (PUNCH-P) reveals cell cycle-specific fluctuations in mRNA translation. Genes Dev. *27*, 1834–1844.

Aviner, R., Hofmann, S., Elman, T., Shenoy, A., Geiger, T., Elkon, R., Ehrlich, M., and Elroy-Stein, O. (2017). Proteomic analysis of polyribosomes identifies splicing factors as potential regulators of translation during mitosis. Nucleic Acids Res. *45*, 5945–5957.

Badertscher, L., Wild, T., Montellese, C., Alexander, L.T., Bammert, L., Sarazova, M., Stebler, M., Csucs, G., Mayer, T.U., Zamboni, N., et al. (2015). Genome-wide RNAi Screening Identifies Protein Modules Required for 40S Subunit Synthesis in Human Cells. Cell Rep. *13*, 2879–2891.

Bashan, A., and Yonath, A. (2008). Correlating ribosome function with high-resolution structures. Trends Microbiol. *16*, 326–335.

Briones, E., Briones, C., Remacha, M., and Ballesta, J.P. (1998). The GTPase center protein L12 is required for correct ribosomal stalk assembly but not for Saccharomyces cerevisiae viability. J. Biol. Chem. *273*, 31956–31961.

Britten, R.J., and Roberts, R.B. (1960). High-Resolution Density Gradient Sedimentation Analysis. Science *131*, 32–33.

Calviello, L., Mukherjee, N., Wyler, E., Zauber, H., Hirsekorn, A., Selbach, M., Landthaler, M., Obermayer, B., and Ohler, U. (2015). Detecting actively translated open reading frames in ribosome profiling data. Nat. Methods *13*, 165–170.

Carpenter, S., Ricci, E.P., Mercier, B.C., Moore, M.J., and Fitzgerald, K.A. (2014). Post-transcriptional regulation of gene expression in innate immunity. Nat. Rev. Immunol. *14*, 361–376.

Chen, S.S., and Williamson, J.R. (2013). Characterization of the Ribosome Biogenesis Landscape in E. coli Using Quantitative Mass Spectrometry. J. Mol. Biol. *425*, 767–779.

Chi, Y., Welcker, M., Hizli, A.A., Posakony, J.J., Aebersold, R., and Clurman, B.E. (2008). Identification of CDK2 substrates in human cell lysates. Genome Biol. *9*, R149.

Cho, J., Chang, H., Kwon, S.C., Kim, B., Kim, Y., Choe, J., Ha, M., Kim, Y.K., and Kim, V.N.

(2012). LIN28A is a suppressor of ER-associated translation in embryonic stem cells. Cell *151*, 765–777.

Chothani, S., Adami, E., Viswanathan, S., Hubner, N., Cook, S., Schafer, S., and Rackham, O. (2017). Reliable detection of translational regulation with Ribo-seq.

Chu, V.T., Van Trung, C., Weber, T., Wefers, B., Wurst, W., Sander, S., Rajewsky, K., and Kühn, R. (2015). Increasing the efficiency of homology-directed repair for CRISPR-Cas9-induced precise gene editing in mammalian cells. Nat. Biotechnol. *33*, 543–548.

Coldwell, M.J., Cowan, J.L., Vlasak, M., Mead, A., Willett, M., Perry, L.S., and Morley, S.J. (2013). Phosphorylation of eIF4GII and 4E-BP1 in response to nocodazole treatment: a reappraisal of translation initiation during mitosis. Cell Cycle *12*, 3615–3628.

Cox, J., and Mann, M. (2008). MaxQuant enables high peptide identification rates, individualized p.p.b.-range mass accuracies and proteome-wide protein quantification. Nat. Biotechnol. *26*, 1367–1372.

Cox, J., Neuhauser, N., Michalski, A., Scheltema, R.A., Olsen, J.V., and Mann, M. (2011). Andromeda: a peptide search engine integrated into the MaxQuant environment. J. Proteome Res. *10*, 1794–1805.

Davis, J.H., Tan, Y.Z., Carragher, B., Potter, C.S., Lyumkis, D., and Williamson, J.R. (2016). Modular Assembly of the Bacterial Large Ribosomal Subunit. Cell *167*, 1610–1622.e15.

Dephoure, N., Zhou, C., Villén, J., Beausoleil, S.A., Bakalarski, C.E., Elledge, S.J., and Gygi, S.P. (2008). A quantitative atlas of mitotic phosphorylation. Proc. Natl. Acad. Sci. U. S. A. *105*, 10762–10767.

Dobin, A., Davis, C.A., Schlesinger, F., Drenkow, J., Zaleski, C., Jha, S., Batut, P., Chaisson, M., and Gingeras, T.R. (2012). STAR: ultrafast universal RNA-seq aligner. Bioinformatics *29*, 15–21.

Edupuganti, R.R., Geiger, S., Lindeboom, R.G.H., Shi, H., Hsu, P.J., Lu, Z., Wang, S.-Y., Baltissen, M.P.A., Jansen, P.W.T.C., Rossa, M., et al. (2017). N(6)-methyladenosine (m(6)A) recruits and repels proteins to regulate mRNA homeostasis. Nat. Struct. Mol. Biol.

Fan, H., and Penman, S. (1970). Regulation of protein synthesis in mammalian cells. II. Inhibition of protein synthesis at the level of initiation during mitosis. J. Mol. Biol. *50*, 655–670.

Ferretti, M.B., Ghalei, H., Ward, E.A., Potts, E.L., and Karbstein, K. (2017). Rps26 directs mRNA-specific translation by recognition of Kozak sequence elements. Nat. Struct. Mol. Biol.

Foster, L.J., de Hoog, C.L., Zhang, Y., Zhang, Y., Xie, X., Mootha, V.K., and Mann, M. (2006). A Mammalian Organelle Map by Protein Correlation Profiling. Cell *125*, 187–199.

Geng, Y., Yu, Q., Sicinska, E., Das, M., Schneider, J.E., Bhattacharya, S., Rideout, W.M., Bronson, R.T., Gardner, H., and Sicinski, P. (2003). Cyclin E Ablation in the Mouse. Cell *114*, 431–443.

Gingold, H., Tehler, D., Christoffersen, N.R., Nielsen, M.M., Asmar, F., Kooistra, S.M., Christophersen, N.S., Christensen, L.L., Borre, M., Sørensen, K.D., et al. (2014). A dual program for translation regulation in cellular proliferation and differentiation. Cell *158*, 1281–

1292.

Gnad, F., Gunawardena, J., and Mann, M. (2011). PHOSIDA 2011: the posttranslational modification database. Nucleic Acids Res. *39*, D253–D260.

Gressner, A.M., and Wool, I.G. (1974). The phosphorylation of liver ribosomal proteins in vivo. Evidence that only a single small subunit protein (S6) is phosphorylated. J. Biol. Chem. *249*, 6917–6925.

Hafner, M., Renwick, N., Farazi, T.A., Mihailović, A., Pena, J.T.G., and Tuschl, T. (2012). Barcoded cDNA library preparation for small RNA profiling by next-generation sequencing. Methods *58*, 164–170.

Havugimana, P.C., Hart, G.T., Nepusz, T., Yang, H., Turinsky, A.L., Li, Z., Wang, P.I., Boutz, D.R., Fong, V., Phanse, S., et al. (2012). A census of human soluble protein complexes. Cell *150*, 1068–1081.

Heide, H., Bleier, L., Steger, M., Ackermann, J., Dröse, S., Schwamb, B., Zörnig, M., Reichert, A.S., Koch, I., Wittig, I., et al. (2012). Complexome profiling identifies TMEM126B as a component of the mitochondrial complex I assembly complex. Cell Metab. *16*, 538–549.

Heyer, E.E., and Moore, M.J. (2016). Redefining the Translational Status of 80S Monosomes. Cell *164*, 757–769.

Holt, L.J., Tuch, B.B., Villén, J., Johnson, A.D., Gygi, S.P., and Morgan, D.O. (2009). Global analysis of Cdk1 substrate phosphorylation sites provides insights into evolution. Science *325*, 1682–1686.

Ingolia, N.T. (2016). Ribosome Footprint Profiling of Translation throughout the Genome. Cell *165*, 22–33.

Ingolia, N.T., Brar, G.A., Rouskin, S., McGeachy, A.M., and Weissman, J.S. (2012). The ribosome profiling strategy for monitoring translation in vivo by deep sequencing of ribosome-protected mRNA fragments. Nat. Protoc. *7*, 1534–1550.

Ishihama, Y., Rappsilber, J., Andersen, J.S., and Mann, M. (2002). Microcolumns with self-assembled particle frits for proteomics. J. Chromatogr. A *979*, 233–239.

Jens, M. (2016). A Pipeline for PAR-CLIP Data Analysis. Methods Mol. Biol. *1358*, 197–207.

Kiick, K.L., Saxon, E., Tirrell, D.A., and Bertozzi, C.R. (2001). Incorporation of azides into recombinant proteins for chemoselective modification by the Staudinger ligation. Proceedings of the National Academy of Sciences *99*, 19–24.

Kristensen, A.R., and Foster, L.J. (2013). High throughput strategies for probing the different organizational levels of protein interaction networks. Mol. Biosyst. *9*, 2201–2212.

Kristensen, A.R., Gsponer, J., and Foster, L.J. (2012). A high-throughput approach for measuring temporal changes in the interactome. Nat. Methods *9*, 907–909.

Kyono, Y., Sugiyama, N., Imami, K., Tomita, M., and Ishihama, Y. (2008). Successive and selective release of phosphorylated peptides captured by hydroxy acid-modified metal oxide chromatography. J. Proteome Res. *7*, 4585–4593.

Langmead, B., and Salzberg, S.L. (2012). Fast gapped-read alignment with Bowtie 2. Nat. Methods *9*, 357–359.

Lauria, F., Tebaldi, T., Bernabo, P., Groen, E.J.N., Gillingwater, T.H., and Viero, G. (2017). riboWaltz: optimization of ribosome P-site positioning in ribosome profiling data.

Lebedeva, S., Jens, M., Theil, K., Schwanhäusser, B., Selbach, M., Landthaler, M., and Rajewsky, N. (2011). Transcriptome-wide analysis of regulatory interactions of the RNA-binding protein HuR. Mol. Cell *43*, 340–352.

Lee, A.S.-Y., Burdeinick-Kerr, R., and Whelan, S.P.J. (2013). A ribosome-specialized translation initiation pathway is required for cap-dependent translation of vesicular stomatitis virus mRNAs. Proc. Natl. Acad. Sci. U. S. A. *110*, 324–329.

Li, F., Long, T., Lu, Y., Ouyang, Q., and Tang, C. (2004). The yeast cell-cycle network is robustly designed. Proc. Natl. Acad. Sci. U. S. A. *101*, 4781–4786.

Liu, F., Rijkers, D.T.S., Post, H., and Heck, A.J.R. (2015). Proteome-wide profiling of protein assemblies by cross-linking mass spectrometry. Nat. Methods *12*, 1179–1184.

Love, M.I., Huber, W., and Anders, S. (2014). Moderated estimation of fold change and dispersion for RNA-seq data with DESeq2. Genome Biol. *15*, 550.

Martin, M. (2011). Cutadapt removes adapter sequences from high-throughput sequencing reads. EMBnet.journal *17*, 10.

Martin, I., Kim, J.W., Lee, B.D., Kang, H.C., Xu, J.-C., Jia, H., Stankowski, J., Kim, M.-S., Zhong, J., Kumar, M., et al. (2014). Ribosomal Protein s15 Phosphorylation Mediates LRRK2 Neurodegeneration in Parkinson's Disease. Cell *157*, 472–485.

Mauro, V.P., and Edelman, G.M. (2002). The ribosome filter hypothesis. Proc. Natl. Acad. Sci. U. S. A. *99*, 12031–12036.

Mauro, V.P., and Matsuda, D. (2016). Translation regulation by ribosomes: Increased complexity and expanded scope. RNA Biol. *13*, 748–755.

Meyuhas, O. (2015). Ribosomal Protein S6 Phosphorylation: Four Decades of Research. Int. Rev. Cell Mol. Biol. *320*, 41–73.

Miyamoto, K., Hara, T., Kobayashi, H., Morisaka, H., Tokuda, D., Horie, K., Koduki, K., Makino, S., Núñez, O., Yang, C., et al. (2008). High-efficiency liquid chromatographic separation utilizing long monolithic silica capillary columns. Anal. Chem. *80*, 8741–8750.

Mudunuri, U., Che, A., Yi, M., and Stephens, R.M. (2009). bioDBnet: the biological database network. Bioinformatics *25*, 555–556.

Olsen, J.V., Blagoev, B., Gnad, F., Macek, B., Kumar, C., Mortensen, P., and Mann, M. (2006). Global, In Vivo, and Site-Specific Phosphorylation Dynamics in Signaling Networks. Cell *127*, 635–648.

Olsen, J.V., Vermeulen, M., Santamaria, A., Kumar, C., Miller, M.L., Jensen, L.J., Gnad, F., Cox, J., Jensen, T.S., Nigg, E.A., et al. (2010). Quantitative phosphoproteomics reveals widespread full phosphorylation site occupancy during mitosis. Sci. Signal. *3*, ra3.

Ong, S.-E., Blagoev, B., Kratchmarova, I., Kristensen, D.B., Steen, H., Pandey, A., and Mann, M. (2002). Stable isotope labeling by amino acids in cell culture, SILAC, as a simple and accurate approach to expression proteomics. Mol. Cell. Proteomics *1*, 376–386.

Ortega, S., Prieto, I., Odajima, J., Martín, A., Dubus, P., Sotillo, R., Barbero, J.L., Malumbres, M., and Barbacid, M. (2003). Cyclin-dependent kinase 2 is essential for meiosis but not for mitotic cell division in mice. Nat. Genet. *35*, 25–31.

Pagliuca, F.W., Collins, M.O., Lichawska, A., Zegerman, P., Choudhary, J.S., and Pines, J. (2011). Quantitative proteomics reveals the basis for the biochemical specificity of the cell-cycle machinery. Mol. Cell *43*, 406–417.

Palozola, K.C., Donahue, G., Liu, H., Grant, G.R., Becker, J.S., Cote, A., Yu, H., Raj, A., and Zaret, K.S. (2017). Mitotic transcription and waves of gene reactivation during mitotic exit. Science *358*, 119–122.

Park, J.-E., Yi, H., Kim, Y., Chang, H., and Kim, V.N. (2016). Regulation of Poly(A) Tail and Translation during the Somatic Cell Cycle. Mol. Cell *62*, 462–471.

Peterson, A.C., Russell, J.D., Bailey, D.J., Westphall, M.S., and Coon, J.J. (2012). Parallel reaction monitoring for high resolution and high mass accuracy quantitative, targeted proteomics. Mol. Cell. Proteomics *11*, 1475–1488.

Presnyak, V., Alhusaini, N., Chen, Y.-H., Martin, S., Morris, N., Kline, N., Olson, S., Weinberg, D., Baker, K.E., Graveley, B.R., et al. (2015). Codon optimality is a major determinant of mRNA stability. Cell *160*, 1111–1124.

Rappsilber, J., Mann, M., and Ishihama, Y. (2007). Protocol for micro-purification, enrichment, pre-fractionation and storage of peptides for proteomics using StageTips. Nat. Protoc. *2*, 1896–1906.

Reschke, M., Clohessy, J.G., Seitzer, N., Goldstein, D.P., Breitkopf, S.B., Schmolze, D.B., Ala, U., Asara, J.M., Beck, A.H., and Pandolfi, P.P. (2013). Characterization and analysis of the composition and dynamics of the mammalian riboproteome. Cell Rep. *4*, 1276–1287.

Ricci, E.P., Kucukural, A., Cenik, C., Mercier, B.C., Singh, G., Heyer, E.E., Ashar-Patel, A., Peng, L., and Moore, M.J. (2014). Staufen1 senses overall transcript secondary structure to regulate translation. Nat. Struct. Mol. Biol. *21*, 26–35.

Roehr, J.T., Dieterich, C., and Reinert, K. (2017). Flexbar 3.0 – SIMD and multicore parallelization. Bioinformatics *33*, 2941–2942.

Ruepp, A., Waegele, B., Lechner, M., Brauner, B., Dunger-Kaltenbach, I., Fobo, G., Frishman, G., Montrone, C., and Mewes, H.-W. (2010). CORUM: the comprehensive resource of mammalian protein complexes--2009. Nucleic Acids Res. *38*, D497–D501.

Ruvinsky, I., Sharon, N., Lerer, T., Cohen, H., Stolovich-Rain, M., Nir, T., Dor, Y., Zisman, P., and Meyuhas, O. (2005). Ribosomal protein S6 phosphorylation is a determinant of cell size and glucose homeostasis. Genes Dev. *19*, 2199–2211.

Sander, S., Calado, D.P., Srinivasan, L., Köchert, K., Zhang, B., Rosolowski, M., Rodig, S.J., Holzmann, K., Stilgenbauer, S., Siebert, R., et al. (2012). Synergy between PI3K signaling and

MYC in Burkitt lymphomagenesis. Cancer Cell *22*, 167–179.

Sander, S., Chu, V.T., Yasuda, T., Franklin, A., Graf, R., Calado, D.P., Li, S., Imami, K., Selbach, M., Di Virgilio, M., et al. (2015). PI3 Kinase and FOXO1 Transcription Factor Activity Differentially Control B Cells in the Germinal Center Light and Dark Zones. Immunity *43*, 1075–1086.

Schmeing, T.M., and Ramakrishnan, V. (2009). What recent ribosome structures have revealed about the mechanism of translation. Nature *461*, 1234–1242.

Schwanhäusser, B., Gossen, M., Dittmar, G., and Selbach, M. (2009). Global analysis of cellular protein translation by pulsed SILAC. Proteomics *9*, 205–209.

Schwanhäusser, B., Busse, D., Li, N., Dittmar, G., Schuchhardt, J., Wolf, J., Chen, W., and Selbach, M. (2011). Global quantification of mammalian gene expression control. Nature *473*, 337–342.

Sengupta, J., Nilsson, J., Gursky, R., Spahn, C.M.T., Nissen, P., and Frank, J. (2004). Identification of the versatile scaffold protein RACK1 on the eukaryotic ribosome by cryo-EM. Nat. Struct. Mol. Biol. *11*, 957–962.

Shi, Z., and Barna, M. (2015). Translating the genome in time and space: specialized ribosomes, RNA regulons, and RNA-binding proteins. Annu. Rev. Cell Dev. Biol. *31*, 31–54.

Shi, Z., Fujii, K., Kovary, K.M., Genuth, N.R., Röst, H.L., Teruel, M.N., and Barna, M. (2017). Heterogeneous Ribosomes Preferentially Translate Distinct Subpools of mRNAs Genome-wide. Mol. Cell.

Shuda, M., Velásquez, C., Cheng, E., Cordek, D.G., Kwun, H.J., Chang, Y., and Moore, P.S. (2015). CDK1 substitutes for mTOR kinase to activate mitotic cap-dependent protein translation. Proc. Natl. Acad. Sci. U. S. A. *112*, 5875–5882.

Simsek, D., and Barna, M. (2017). An emerging role for the ribosome as a nexus for post-translational modifications. Curr. Opin. Cell Biol. *45*, 92–101.

Simsek, D., Tiu, G.C., Flynn, R.A., Byeon, G.W., Leppek, K., Xu, A.F., Chang, H.Y., and Barna, M. (2017). The Mammalian Ribo-interactome Reveals Ribosome Functional Diversity and Heterogeneity. Cell *169*, 1051–1065.e18.

Slavov, N., Semrau, S., Airoldi, E., Budnik, B., and van Oudenaarden, A. (2015). Differential Stoichiometry among Core Ribosomal Proteins. Cell Rep. *13*, 865–873.

Sonenberg, N., and Hinnebusch, A.G. (2009). Regulation of Translation Initiation in Eukaryotes: Mechanisms and Biological Targets. Cell *136*, 731–745.

Spahn, C.M.T., Gomez-Lorenzo, M.G., Grassucci, R.A., Jørgensen, R., Andersen, G.R., Beckmann, R., Penczek, P.A., Ballesta, J.P.G., and Frank, J. (2004). Domain movements of elongation factor eEF2 and the eukaryotic 80S ribosome facilitate tRNA translocation. EMBO J. *23*, 1008–1019.

Spence, J., Gali, R.R., Dittmar, G., Sherman, F., Karin, M., and Finley, D. (2000). Cell Cycle–Regulated Modification of the Ribosome by a Variant Multiubiquitin Chain. Cell *102*, 67–76.

Steitz, T.A. (2008). A structural understanding of the dynamic ribosome machine. Nat. Rev. Mol. Cell Biol. *9*, 242–253.

Stumpf, C.R., Moreno, M.V., Olshen, A.B., Taylor, B.S., and Ruggero, D. (2013). The Translational Landscape of the Mammalian Cell Cycle. Mol. Cell *52*, 574–582.

Szklarczyk, D., Morris, J.H., Cook, H., Kuhn, M., Wyder, S., Simonovic, M., Santos, A., Doncheva, N.T., Roth, A., Bork, P., et al. (2017). The STRING database in 2017: quality-controlled protein-protein association networks, made broadly accessible. Nucleic Acids Res. *45*, D362–D368.

Tanenbaum, M.E., Stern-Ginossar, N., Weissman, J.S., and Vale, R.D. (2015). Regulation of mRNA translation during mitosis. Elife *4*.

Taylor, D., Unbehaun, A., Li, W., Das, S., Lei, J., Liao, H.Y., Grassucci, R.A., Pestova, T.V., and Frank, J. (2012). Cryo-EM structure of the mammalian eukaryotic release factor eRF1-eRF3-associated termination complex. Proc. Natl. Acad. Sci. U. S. A. *109*, 18413–18418.

Thompson, M.K., Rojas-Duran, M.F., Gangaramani, P., and Gilbert, W.V. (2016). The ribosomal protein Asc1/RACK1 is required for efficient translation of short mRNAs. Elife *5*.

Toprak, U.H., Gillet, L.C., Maiolica, A., Navarro, P., Leitner, A., and Aebersold, R. (2014). Conserved Peptide Fragmentation as a Benchmarking Tool for Mass Spectrometers and a Discriminating Feature for Targeted Proteomics. Mol. Cell. Proteomics *13*, 2056–2071.

Tripathi, S., Pohl, M.O., Zhou, Y., Rodriguez-Frandsen, A., Wang, G., Stein, D.A., Moulton, H.M., DeJesus, P., Che, J., Mulder, L.C.F., et al. (2015). Meta- and Orthogonal Integration of Influenza "OMICs" Data Defines a Role for UBR4 in Virus Budding. Cell Host Microbe *18*, 723–735.

Truitt, M.L., and Ruggero, D. (2017). New frontiers in translational control of the cancer genome. Nat. Rev. Cancer *17*, 332.

Veit, G., Oliver, K., Apaja, P.M., Perdomo, D., Bidaud-Meynard, A., Lin, S.-T., Guo, J., Icyuz, M., Sorscher, E.J., Hartman, J.L., IV, et al. (2016). Ribosomal Stalk Protein Silencing Partially Corrects the ΔF508-CFTR Functional Expression Defect. PLoS Biol. *14*, e1002462.

Voorhees, R.M., Fernández, I.S., Scheres, S.H.W., and Hegde, R.S. (2014). Structure of the mammalian ribosome-Sec61 complex to 3.4 Å resolution. Cell *157*, 1632–1643.

Wang, X., Zhao, B.S., Roundtree, I.A., Lu, Z., Han, D., Ma, H., Weng, X., Chen, K., Shi, H., and He, C. (2015). N(6)-methyladenosine Modulates Messenger RNA Translation Efficiency. Cell *161*, 1388–1399.

Wawiórka, L., Molestak, E., Szajwaj, M., Michalec-Wawiórka, B., Boguszewska, A., Borkiewicz, L., Liudkovska, V., Kufel, J., and Tchórzewski, M. (2016). Functional analysis of the uL11 protein impact on translational machinery. Cell Cycle *15*, 1060–1072.

Wild, T., Horvath, P., Wyler, E., Widmann, B., Badertscher, L., Zemp, I., Kozak, K., Csucs, G., Lund, E., and Kutay, U. (2010). A protein inventory of human ribosome biogenesis reveals an essential function of exportin 5 in 60S subunit export. PLoS Biol. *8*, e1000522.

Wilhelm, M., Schlegl, J., Hahne, H., Gholami, A.M., Lieberenz, M., Savitski, M.M., Ziegler, E.,

Butzmann, L., Gessulat, S., Marx, H., et al. (2014). Mass-spectrometry-based draft of the human proteome. Nature *509*, 582–587.

Wilker, E.W., van Vugt, M.A.T.M., Artim, S.A., Huang, P.H., Petersen, C.P., Reinhardt, H.C., Feng, Y., Sharp, P.A., Sonenberg, N., White, F.M., et al. (2007). 14-3-3sigma controls mitotic translation to facilitate cytokinesis. Nature *446*, 329–332.

Xue, S., Tian, S., Fujii, K., Kladwang, W., Das, R., and Barna, M. (2014). RNA regulons in Hox *5′* UTRs confer ribosome specificity to gene regulation. Nature *517*, 33–38.

Zauber, H., Kirchner, M., and Selbach, M. (2018). Picky: a simple online PRM and SRM method designer for targeted proteomics. Nat. Methods *15*, 156–157.

Zhu, H., and Mao, Y. (2015). Robustness of cell cycle control and flexible orders of signaling events. Sci. Rep. *5*, 14627.

Main figure titles and legends

Figure 1. Polysome proteome profiling (3P)

(A) Experimental design for 3P. (B) Exemplary spectra for two peptides across fractions, one for a small (RPS25/eS25) and one for a large (RPL8/uL2) subunit protein. Fraction numbers are like in panel D. (C) Hierarchical clustering for 1,609 proteins quantified in more than 10 fractions in at least one cell line. Columns refer to density gradient fractions (from fraction 1 to 36). Rows represent individual proteins. (D) Abundance profiles for individual ribosomal proteins across density gradient (shown for HEK293 replicate 2 as an example). The corresponding UV absorbance profile at 254 nm (dominated by ribosomal RNA) is shown in the top right corner of the figure.

Figure 2. Mapping polysome interacting proteins

(A) Top: Overlap of proteins (excluding ribosomal proteins) identified in polysome fractions in our study and the so-called "mammalian riboproteome". Bottom: Complexes with cytosolic RPs (green bars, including ribosomal proteins) and several non-ribosomal complexes (purple bars) are significantly enriched. (B) To identify ribosome-associated proteins profiles of individual proteins are compared to the polysome consensus profile by computing MSD values. (C) Observed distribution of MSD values in HEK293 (green). Cytosolic (red) and mitochondrial RPs (purple) can be easily separated. The MSD value distribution of an exemplarily shuffled dataset is depicted in grey. Multiple shuffling operations were used to define cut-offs (nominal FDR=0). Insets show reproducibility of MSD values between replicates. (D) Same as in (A) but only using proteins that pass the MSD cut-off (i.e. polysome-associated proteins). (E) Receiver-operator characteristic (ROC) curves for our data compared to a reference dataset. Red and green ROC curves depict polysome interactomes with and without cytosolic RPs, respectively. (F) Top: Overlap of polysome-associated proteins in HEK293 and HeLa. Bottom: Enriched GO terms among the 145 polysome associated proteins (adjusted $P<0.01$). (G) Fractions of proteins with ribosome-related annotations for different subsets. (H) Absolute abundance estimates of cytosolic RPs and polysome-associated proteins. (I) Abundance profiles for three known polysome interactors. (J) Scatter plot of MSD values calculated from 40S fractions (x-axis) and 60S fractions (y-axis) in HEK293 (see Figure S3C for HeLa). Fractions of 40S-associated, 60S-associated and unassigned proteins are shown in the top right corner.

Figure 3. Phosphorylation profile of RPs

(A) Quantified phosphorylation sites of RPs mapped to the ribosome structure (PDB: 4V6X; (Anger et al., 2013). Phosphorylated RPSs and RPLs are shown in blue and red, respectively. An enlarged view of the P stalk shows that RPL12/uL11 pS38 is proximal to the ribosomal GTPase EEF2. (B) MSD values of phosphosites indicate that phosphorylation of most sites does not significantly vary across complexes. RPL12/uL11 pS38 (red) shows the largest divergence from consensus profiles. (C) Profile for RPS6/eS6 in HeLa cells. Blue and red lines indicate consensus profiles of 40S and 60S proteins, respectively. Abundance of RPS6/eS6-derived phosphopeptides are shown as gray bars. (D) Profiles for RPL12/uL11 pS38 in HeLa (left). Representative MS spectra from fractions 9-10 and 31-32 (second panel), a representative MS/MS spectrum of RPL12/uL11 pS38 (third panel) and profiles for RPL12/uL11 pS38 in HEK293 (right panel) are also shown. (E) Western blots of whole cell lysates from HEK293 cells stably expressing FLAG/HA-tagged RPL12/uL11_WT, S38D or S38A.

Figure 4. Impact of RPL12/uL11 pS38 on global protein synthesis

(A) Conservation and phosphorylation motif of RPL12/uL11 S38. (B) Phosphorylation of S38 during the cell cycle in published phosphoproteomic data. (C) Experimental design for flow cytometric analysis of mitotic translation in HEK293 cells transiently expressing FLAG/HA tagged RPL12/uL11. (D) Monitoring global protein synthesis in interphase and mitotis. Left: Representative FACS result of cells expressing FLAG/HA RPL12/uL11 WT. Only cells expressing tagged RPL12/uL11 were gated and the corresponding cell population was further analyzed by dual staining for phospho H3 S10 and AHA-labeled proteins. Global protein synthesis was monitored by AHA incorporation (y-axis) in interphase and mitosis (based on H3 pS10 staining, x-axis). Right: Each dot represents median AHA intensity calculated from interphase or mitotic cell population in an independent experiment. The results from three independent experiments are shown. As controls, methionine (Met) incorporation into proteins instead of AHA and protein production in the presence of CHX were also monitored. (E) Mitotic index determined by flow cytometric analysis of H3 pS10-positive cells expressing tagged RPL12/uL11. Data are represented as mean ± SD. P-values were calculated using paired student's t test.

Figure 5. Role for RPL12/uL11 pS38 in mitotic translation

(A) pSILAC quantifies differences in protein production between RPL12/uL11 S38D- and S38A-expressing cells. Left: Experimental design. Right: Cumulative distribution of log2-fold changes (H/M ratios) of protein synthesis. Subsets of proteins whose mRNAs exhibited higher (>2-fold)

or lower (<0.5-fold) ribosome occupancy in mitosis than in S phase (Stumpf et al., 2013) is shown in light red and light green, respectively. All quantified proteins are shown in gray. P-values were computed using one-sided Wilcoxon-rank sum tests. (B) RNA-seq analysis of monosome-bound mRNAs. Left: Monosomes were isolated by sucrose density gradient centrifugation from HEK293 cells stably expressing FLAG/HA RPL12/uL11, followed by anti-FLAG immunoprecipitation to enrich for tagged RPL12/uL11-containing ribosomes. Poly(A)+ RNAs from the monosome fraction (input) and anti-FLAG immunoprecipitated fraction (IP) were quantified by RNA-seq. Only mRNAs that exhibited positive enrichment values (IP/input > 0) were used for further analysis (see Figure S3C). Right: Cumulative distribution of log2 fold-changes in ribosome occupancy (mitosis vs S phase, taken from Stumpf et al) for 3 classes of mRNAs with high, medium and low enrichment ratios (S38D vs S38A). P-values were computed using one-sided Wilcoxon-rank sum tests. (C) GO enrichment analysis for genes that showed high S38D/S38A enrichment in the RNA-seq experiment (see Figure 5B). Adjusted p-values by Benjamini–Hochberg are shown. (D) Barplots showing correlation coefficient between codon frequencies within coding sequences and the observed differences in enrichment ratios (S38D/S38A) for all 64 possible triplets. Light red and light blue indicate codons ending in A/U and G/C, respectively. (E) Correlation between GC content within coding sequences and the observed differences in enrichment ratios(S38D/S38A). (F) Mitotically transcribed mRNAs preferentially associate with monosomes carrying the S38D mutant. Boxplots showing changes in enrichment ratios (S38D/S38A) for three subsets, "transcribed in mitosis (pink)", "transcriptionally induced in mitosis (light blue)" and "other (orange)", based on the dataset from (Palozola et al., 2017). P-values were computed using Mann-Whitney U test. (G) Density plots of GC contents for the three subsets based on (Palozola et al., 2017).

Figure 6. Translational regulation through RPL12 pS38 in mouse B cells

(A) Monitoring global protein synthesis in interphase and mitotic cells. Left: Each dot represents median AHA intensity calculated from interphase or mitotic cell population in an independent experiment. The results from three independent experiments are shown. As a negative control, methionine (Met) incorporation into proteins was also monitored instead of AHA. Right: Mitotic index determined by flow cytometric analysis of H3 pS10-positive cells. Data are represented as mean ± SD. P-values were calculated using paired Student's t test. (B) A pSILAC approach to assess the difference in protein production between the S38D and the S38A mutant cells. Cumulative distribution of log2-fold changes (H/M ratios) of protein synthesis in asynchronous cells is shown (see also Figure S6A for the label-swap experiment). Subsets of proteins whose

mRNAs exhibited higher (>2-fold) or lower (<0.5-fold) ribosome occupancy in mitosis than in S phase (Stumpf et al., 2013) are shown in light red and light green, respectively. Subsets of proteins that exhibited higher (>1.4-fold) or lower (<0.7-fold) ibosome protected fragments (RPFs) in mitotic versus asynchronous B cells (our ribosome profiling data, see also Figure S6) are shown in red and dark green, respectively. All quantified proteins are shown in gray. P-values were computed using one-sided Wilcoxon-rank sum tests. (C) Boxplots comparing pSILAC (Figure 6B) and ribosome profiling (Figure 6D) for the subsets based on log2 fold-changes (S38D/S38A) of the pSILAC data. Changes in RPFs were calculated from our own Ribo-seq libraries. P-values were computed using one-sided Wilcoxon-rank sum tests. (D) Cumulative distribution of log2-fold changes (S38A/S38D) in RPFs in asynchronous cells. Subsets are based on our ribosome profiling data (see legend to panel B above). P-values were computed using one-sided Wilcoxon-rank sum tests.

STAR*METHODS

Detailed methods are provided in the online version of this paper and include the following:

- KEY RESOURCES TABLE
- CONTACT FOR REAGENT AND RESOURCE SHARING
- EXPERIMENTAL MODEL AND SUBJECT DETAILS: Cell Lines
- METHOD DETAILS
    - Sucrose Density Gradient Centrifugation
    - Sample Preparation for Proteome Analysis
    - Phosphopeptide Enrichment
    - NanoLC-MS/MS Analysis
    - Parallel Reaction Monitoring (PRM) assay
    - Processing of Mass Spectrometry Data
    - Data Analysis of PRM Measurements
    - Estimation of Protein Abundance Using iBAQ
    - Generation of HEK293 Stable Cell Lines Expressing FLAG/HA-RPL12
    - Generation of RPL12 Point Mutant Cell Lines via CRISPR/Cas9
    - Western Blotting of Sucrose Density Gradient Fractions
    - AHA Labeling and Flow Cytometric Analysis
    - Pulsed SILAC (pSILAC)
    - Immunoprecipitation of FLAG/HA-tagged RPL12 from Sucrose Gradient Fractions and Library Preparation
    - RNA-seq Data Processing and Analysis
    - Ribosome Profiling for Mouse B cells
    - Ribosome Profiling Data Processing and Analysis
    - Identifying ribosome-associated proteins using MSD
    - Protein Complex Enrichment Analysis

- QUANTIFICATION AND STATISTICAL ANALYSIS
- DATA AND SOFTWARE AVAILABILITY
    - Data Resources

KEY RESOURCES TABLE

REAGENT or RESOURCE	SOURCE	IDENTIFIER

Antibodies		
Rabbit polyclonal anti-HA	Santa Cruz	Cat# sc-805 RRID:AB_631618
Rabbit polyclonal anti-RPL12	Thermo Fisher Scientific	Cat#PA5-31670 RRID:AB_2549143
Rabbit monoclonal anti-RPL12 (Center)	Abgent	Cat# WA-AP16275c RRID:AB_11135986
Rabbit polyclonal anti-RPS5	Bethyl Laboratories	Cat#A304-011A RRID:AB_2620359
Rabbit polyclonal anti-NUFIP2/82-FIP antibody	Bethyl Laboratories	Cat# A301-600A RRID:AB_1078870
Rabbit polyclonal anti-GPATCH4 antibody	Bethyl Laboratories	Cat# A303-405A RRID:AB_10954002
Rabbit polyclonal anti-LLPH antibody	Sigma-Aldrich	Cat# SAB1302290
Rabbit polyclonal anti-UQCRC2 antibody	GeneTex	Cat# GTX114873 RRID:AB_11164243
Rabbit polyclonal anti-H1FX antibody	Aviva	Cat# ASB-OAAB10031
Rabbit polyclonal anti-C11orf48 antibody	Origene	Cat# TA331749
Rabbit polyclonal anti-C7orf50 antibody	Proteintech	Cat# 20797-1-AP RRID:AB_10732839
Rabbit monoclonal phospho-Histone H3 (Ser10) (D2C8) (Alexa Fluor 647 conjugate) antibody	Cell Signaling Technology	Cat# 3458S RRID:AB_10694086
Monoclonal anti-DYKDDDK-Biotin	Miltenyi Biotec	Cat# 130-101-569
Mouse monoclonal anti-FLAG (M2)	Sigma-Aldrich	Cat# F3165 RRID:AB_259529
Rat monoclonal PE/Cy7 Streptavidin	Biolegend	Cat# BLD-405206
Sheep anti-mouse IgG-HRP	Sigma-Aldrich	Cat# NA931 RRID:AB_772210

Donkey anti-rabbit IgG-HRP	Sigma-Aldrich	Cat# NA934 RRID:AB_772206
Chemicals, Peptides, and Recombinant Proteins		
Cycloheximide	Sigma-Aldrich	Cat#C4859; CAS: 66-81-9
nocodazole	Sigma-Aldrich	Cat#M1404; CAS: 31430-18-9
L-Azidohomoalanine (AHA)	Anaspec	Cat#AS-63699
L-Lysine 4,4,5,5-D4 (Lys4)	Cambridge Isotope Laboratories	Cat#DLM-2640
L-Lysine $^{13}C_6$ $^{15}N_2$ (Lys8)	Cambridge Isotope Laboratories	Cat#CNLM-291-H
L-Arginine $^{13}C_6$ (Arg6)	Sigma-Aldrich	Cat#643440
L-Arginine $^{13}C_6{}^{15}N_4$ (Arg10)	Sigma-Aldrich	Cat#608033
Alexa Fluor 488 alkyne	Thermo Fisher Scientific	Cat#A10267
Trizol	Thermo Fisher Scientific	Cat#15596026
Trizol LS	Thermo Fisher Scientific	Cat#10296028
ERCC Spike-in Control Mix 1	Thermo Fisher Scientific	Cat#4456740
TurboDNase	Thermo Fisher Scientific	Cat#AM2239
RNase I	Thermo Fisher Scientific	Cat#AM2295
SUPERaseIn	Thermo Fisher Scientific	Cat#AM2696
Critical Commercial Assays		
Truseq stranded mRNA kit	Illumina	Cat#20020594
RNA Clean and Concentrator kit	Zymo Research	Cat#R1013
RiboZero Kit	Illumina	Cat#MRZH11124
QuantSeq 3' mRNA-Seq Library Prep Kit FWD	Lexogen	Cat#SKU: 015.24.
Deposited Data		

Proteomic datasets	This paper	Polysome (phospho)proteome profiling for HEK293 and HeLa ProteomeXchange: PXD009292; Polysome proteome profiling for mESC ProteomeXchange: PXD009268; pSILAC in HEK293 ProteomeXchange: PXD009307; Polysome proteome profiling for B cells ProteomeXchange: PXD009267; pSILAC in B cells ProteomeXchange: PXD009276; PRM assay in B cells ProteomeXchange: PXD010029
RNA-seq and ribo-seq datasets	This paper	GEO: GSE112187
Human UniprotKB/Swiss-Prot data base (Human UniProt 2014-10)	N/A	http://www.uniprot.org/proteomes/
Mouse UniprotKB/Swiss-Prot data base (Mouse UniProt 2014-10)	N/A	http://www.uniprot.org/proteomes/
Riboproteome data	(Reschke et al., 2013)	N/A
Ribosome profiling data (mitosis vs S phase)	(Stumpf et al., 2013)	N/A
Protein complex annotation data (CORUM downloaded Jan/2017)	(Ruepp et al., 2010)	http://mips.helmholtz-muenchen.de/genre/proj/corum/index.htmL
STRING protein interaction database	(Szklarczyk et al., 2017)	https://string-db.org/
RNAi data for ribosome biogenesis proteins	(Badertscher et al., 2015; Wild et al., 2010)	N/A

Experimental Models: Cell Lines		
Human HeLa cells	ATCC	N/A
Human HEK293 cells	ATCC	CRL-1573
NIH 3T3 mouse fibroblast cells	ATCC	N/A
Mouse embryonic stem cells (E14)	Michel Vermeulen (Radboud Institute for Molecular Life Sciences	N/A
Flp-In T-REx 293 Cell Line	Thermo Fisher Scientific	R78007
19DN mouse B cells and RPL12 mutant cells	(Sander et al., 2012) and this paper	N/A
Oligonucleotides		
oligonucleotides used for genome editing, see "Generation of RPL12 Point Mutant Cell Lines via CRISPR/Cas9"	This paper	N/A
Recombinant DNA		
pDONR221	Thermo Fisher Scientific	Cat#12536017
pDEST26_FLAG/HA	This paper	N/A
pcDNA5-FLAG/HA-RPL12-WT	This paper	N/A
pcDNA5-FLAG/HA-RPL12-S38D	This paper	N/A
pcDNA5-FLAG/HA-RPL12-S38A	This paper	N/A
pFRT/TO/FLAG/HA-DEST	Thomas Tuschl	Addgene ID: 26360
pX330-Cas9-RPL12sgRNA	This paper	N/A
pX330-E2A-mCherry	(Chu et al., 2015)	N/A
Software and Algorithms		

R studio version 1.1.4	N/A	https://www.rstudio.com
MaxQuant v1.5.1.2	(Cox and Mann, 2008)	http://www.biochem.mpg.de/5111795/maxquant
Metascape	(Tripathi et al., 2015)	http://metascape.org/
Bcl2Fastq (v2.16.0.10)	Illumina	https://support.illumina.com/sequencing/sequencing_software/bcl2fastq-conversion-software.htmL
Flexbar (v2.5)	(Roehr et al., 2017)	https://github.com/seqan/flexbar/wiki
collapse_reads.pl script	(Jens, 2016)	https://github.com/marvin-jens/clip_analysis
STAR aligner v2.4.2a, v2.5.3a	(Dobin et al., 2012)	https://github.com/alexdobin/STAR
DESeq2 (v1.18.1)	(Love et al., 2014)	https://bioconductor.org/packages/release/bioc/htmL/DESeq2.htmL
FASTX Toolkit (v0.0.14)	N/A	http://hannonlab.cshl.edu/fastx_toolkit/
Bowtie 2 (v2.3.2)	(Langmead and Salzberg, 2012)	http://bowtie-bio.sourceforge.net/bowtie2/index.shtmL
HTSeq-count (v0.9.1)	(Anders et al., 2014)	http://htseq.readthedocs.io/en/master/count.htmL
Detection of differential translation genes (DTGs) using DESeq2 interaction term	(Chothani et al., 2017)	https://github.com/SGDDNB/DTG-detection/blob/master/getDTG.md
cutadapt (v.1.12)	(Martin, 2011)	http://cutadapt.readthedocs.io/en/stable/guide.htmL
riboWaltz (v.0.1.0)	(Lauria et al., 2017)	https://github.com/LabTranslationalArchitectomics/riboWaltz
RiboTaper (v1.3)	(Calviello et al., 2015)	https://ohlerlab.mdc-berlin.de/software/RiboTaper_126/
Other		

Titansphere	GL Sciences	Cat#5010-21315
MonoCap C18 High Resolution 2000	GL Sciences	Cat#5020-10015
Dynabeads Protein G	Thermo Fisher Scientific	Cat#10004D
MicroSpin S-400 HR Columns	GE Healthcare	Cat#27-5140-01

CONTACT FOR REAGENT AND RESOURCE SHARING

Further information and requests for reagents may be directed to, and will be fulfilled by the corresponding authors, Koshi Imami (imami.koshi.3z@kyoto-u.ac.jp) or Matthias Selbach (matthias.selbach@mdc-berlin.de).

EXPERIMENTAL MODEL AND SUBJECT DETAILS

Cell Lines

HEK293, HeLa and NIH3T3 cells (American Type Culture Collection) were cultured in Dulbecco's modified Eagle's medium (DMEM) (life technologies) complemented with glutamax (life technologies) and 10% fetal bovine serum (FBS) (PAN-Biotech). For SILAC labeling, cells were grown in arginine- and lysine-free DMEM (life technologies) containing 10% (v/v) dialyzed FBS (Pan-Biotech), 1% glutamax (life technologies), 1% sodium pyruvate (life technologies) in the presence of either 0.2 mM L-arginine (Sigma-Aldrich) and 0.8 mM L-lysine ("light" form) (Sigma-Aldrich), L-[$^{13}C_6$]-arginine (Sigma-Aldrich) and L-[$^{2}H_4$]-lysine ("medium-heavy" form) (Cambridge Isotope Laboratories) or L-[$^{13}C_6$,$^{15}N_4$]-arginine (Sigma-Aldrich) and L-[$^{13}C_6$,$^{15}N_2$]-lysine ("heavy" form) (Cambridge Isotope Laboratories). To achieve complete incorporation of SILAC amino acids, cells were cultured in a SILAC medium for at least five doubling and labeling efficiency was confirmed by a mass spectrometry.

Mouse embryonic stem cells (E14, 6th passage) were kindly provided from Michel Vermeulen lab (Radboud Institute for Molecular Life Sciences) and cultured in collagen coated plates with DMEM high glucose media (life technologies) supplemented with 15% mESC compatible FBS (Hyclone cat no. SV30180.03, lot SZB20006), 1% non-essential amino acids (life technologies), 0.1 mM ß-mercaptoethanol (Sigma-Aldrich), 1% penicillin and streptomycin (life technologies), leukemia inhibitory factor (LIF; 1,000 U/mL) (ESG1107, Merk Millipore) and 2i (3 µM CHIR99021 and 1 µM PD0325901) (130-104-170, Miltenyi Biotec). For the polysome proteome profiling, 11 th passage cells were used.

Murine B cell lymphoma line, 19PP, was established from Rag2-/-γC-/- mouse reconstituted with Cγ1-Cre; Myc/P110*flSTOP mouse BM cells (Sander et al., 2012). 19PP cells were transfected with Flp-expressing plasmid to delete GFP and hCD2 reporter genes. Reporter negative subline, 19DN, was established by FACS sorting of reporter double-negative 19PP cells. 19DN cells were maintained in DMEM medium (Gibco) containing 10% heat inactivated FBS, glutamax, sodium pyruvate, HEPES, non-essential amino acids, penicillin streptomycin (all 1%) and 52 µM β-mercaptoethanol.

METHOD DETAILS

Sucrose Density Gradient Centrifugation

On day of experiment, cells were grown to 80% confluency (one 15 cm plate per condition) and incubated with cycloheximide (CHX, 100 µg/mL) for 5 min at 37 ^{o}C before harvesting. Cells were washed with ice cold PBS containing CHX (100 µg/mL) and lysed with 300 µL of polysome lysis buffer [10 mM HEPES pH 7.4, 150 mM KCl, 5 mM $MgCl_2$, 0.5 mM DTT, 0.5% NP-40, EDTA-free protease inhibitor cocktail (Roche), SUPERaseIn (Thermo Fischer Scientific, AM2696, 20 U/µL) and 100 µg/mL CHX)]. After lysing the cells by passing ten times through 21 gauge needle, cell debris was removed by centrifugation (20,000 g, 10 min, 4 ^{o}C). The supernatant was then layered onto a 10 mL linear sucrose gradient 15–45% (w/v), supplemented with 10 mM HEPES pH 7.4, 150 mM KCl, 5 mM $MgCl_2$, 0.5 mM DTT and 100 µg/mL CHX and centrifuged (36,000 rpm, 150 min, 4°C) using a Sorvall WX 90 ultracentrifuge (Thermo Fisher Scientific). Approximately 40 fractions (250 µL each) from each condition were collected using a gradient station (Biocomp). For polysome proteome profiling by mass spectrometry, cell lysates from different labeling states were individually resolved by density gradient centrifugation. Each individual fraction from light and heavy cells were combined as biological duplicate. For medium-heavy cells, all fractions were pooled and subsequently spiked-in each fraction from the combined light and heavy mixtures as an internal standard. For the polysome proteome profiling of mESCs, heavy-labeled NIH3T3 cells were used an internal standard (see Figure S1) as cell culture medium and serum for SILAC labeling of mESCs are not commercially available.

Sample Preparation for Proteome Analysis

Proteins from the fractionated samples were precipitated with 20% trichloroacetic acid (TCA) and the precipitated pellets were washed three times with ice-cold acetone. The remaining

solution was evaporated by a speedvac (Eppendorf™ Vacufuge™ Concentrator). Protein pellets were resuspended in 50 µL of 8 M urea and 0.1 M Tris-HCl, pH 8. Proteins were reduced with 10 mM dithiothreitol (DTT) at room temperature for 30 min and alkylated with 50 mM iodoacetamide (IAA) at room temperature for 30 min in the dark room. Proteins were first digested by lysyl endopeptidase (LysC) (Wako) at a protein-to-LysC ratio of 100:1 (w/w) at room temperature for 3 hr. Then, the sample solution was diluted to final concentration of 2 M urea with 50 mM ammonium bicarbonate (ABC). Trypsin (Promega) digestion was performed at a protein-to-trypsin ratio of 100:1 (w/w) under constant agitation at room temperature for 16 hr. Peptides were desalted with C18 Stage tips and further cleaned up with SCX (strong cation exchange chromatography) Stage tips and desalted again with C18 Stage tips (Rappsilber et al., 2007) prior to LC-MS/MS analysis.

For other standard proteome samples, cells were lysed in 50 µL of 8 M urea and 0.1 M Tris-HCl, pH 8. Protein reduction, alkylation and digestion were performed as described above. Peptides were desalted with a C18 Stage tip before LC-MS/MS analysis.

Phosphopeptide Enrichment

For the density gradient samples are exactly same as the ones used for polysome proteome profiling (see "Sucrose Density Gradient Centrifugation"), two adjacent fractions were combined in order to increase starting material for phosphopeptide enrichment. Peptides were resuspended in 100 µL of loading buffer [80% ACN (vol/vol) and 6% TFA (vol/vol)]. Phosphopeptides were enriched using a microcolumn tip packed with 0.5 mg of TiO_2 (Titansphere, GL Sciences) (Rappsilber et al., 2007) and following steps were performed at 4 ^{o}C. The TiO_2 tips were equilibrated with 20 µL of the loading buffer via centrifugation of 100 g. 50 µL of the sample solution was loaded on a TiO_2 tip via centrifugation of 100 g and this step was repeated until the sample solution was completely loaded. The TiO_2 column was washed with 20 µL of the loading buffer, followed by 20 µL of washing buffer [50% ACN (vol/vol) and 0.1% TFA (vol/vol)]. The bound phosphopeptides were eluted using successive elution with 30 µL of elution buffer 1 (5% ammonia solution), followed by 30 µL of elution buffer 2 (5% piperidine) (Kyono et al., 2008). Each fraction was collected into a fresh tube containing 30 µL of 20% formic acid. 3 µL of 100% formic acid was added to further acidify the samples. The phosphopeptides were desalted with C18 Stage Tips prior to LC-MS/MS analysis.

NanoLC-MS/MS Analysis

Reversed-phase liquid chromatography was performed by employing an EASY nLC II , 1000 or 1200 (Thermo Fisher Scientific) using self-made fritless C18 microcolumns (Ishihama et al., 2002) (75 µm ID packed with ReproSil-Pur C18-AQ 3-µm resin, Dr. Maisch GmbH) connected on-line to the electrospray ion source (Proxeon) of a Q Exactive mass spectrometer or Q Exactive plus (Thermo Fisher Scientific). The mobile phases consisted of (A) 0.1% formic acid and 5% acetonitrile and (B) 0.1% formic acid and 80% acetonitrile. For the fractionated samples, peptides were eluted from the analytical column at a flow rate of 200 nL/min by altering the gradient: 5-6% B in 2 min, 6-8% B in 14 min, 8-20% B in 44 min, 20-33% in 50 min, 33-45% B in 12 min, 45-60% B in 2 min and 60-95% B in 1 min. Phosphopeptides were separated on a 2 m monolithic column (Miyamoto et al., 2008) [MonoCap C18 High Resolution 2000 (GL Sciences), 100 mm i.d. x 2,000 mm] at a flow rate of 300 nL/min by altering the gradient: 5-6% B in 2 min, 6-8% B in 18 min, 8-20% B in 80 min, 20-33% in 80 min, 33-45% B in 20 min, 45-60% B in 2 min, 60-95% B in 1 min. The Q Exactive (plus) instrument was operated in the data dependent mode with a full scan in the Orbitrap followed by top 10 MS/MS scans using higher-energy collision dissociation (HCD). For standard proteome analyses, the full scans were performed with a resolution of 70,000, a target value of $3x10^6$ ions and a maximum injection time of 20 ms. The MS/MS scans were performed with a 17,500 resolution, a $1x10^6$ target value and a 60 ms maximum injection time. For phosphoproteome analyses, the full scans were performed with a resolution of 70,000, a target value of $3x10^6$ ions and a maximum injection time of 120 ms. The MS/MS scans were performed with a 35,000 resolution, a $5x10^5$ target value and a 160 ms maximum injection time. Isolation window was set to 2 and normalized collision energy was 26. Ions with an unassigned charge state and singly charged ions were rejected. Former target ions selected for MS/MS were dynamically excluded for 30 s.

Parallel Reaction Monitoring (PRM) assay

50 randomly selected proteins from the shotgun experiment with log2 fold changes > 0.1 and < -0.1 were selected to be reanalyzed with PRM (Peterson et al., 2012) (see Table S5 for the complete list). We additionally included a set of 10 proteins within the range of -0.2 and 0.2 log2 fold change that served as an internal control. The inclusion list for the PRM method was generated using Picky (Zauber et al., 2018) with SILAC option enabled (including Lys4 and Arg6 as medium-heavy and Lys8 and Arg10 as heavy label), a retention time window of 50 min and setting the species to mouse. Predicted retention-times were calibrated in Picky with a complex sample of tryptically digested *E. coli* proteome immediately before the start of the PRM

measurements. Peptides were separated by reverse phase chromatography on an effective 200 min gradient and analyzed on a Q-Exactive HFx (Thermo Fisher Scientific). The PRM settings were: 15,000 resolution; $2x10^5$ AGC target; 1.6 m/z isolation window; 40 ms maximum ion injection time.

Processing of Mass Spectrometry Data

All raw data were analyzed and processed by MaxQuant (v1.5.1.2) (Cox and Mann, 2008). Default settings were kept except that 'match between runs' was turned on. Search parameters included two missed cleavage sites, cysteine carbamidomethyl fixed modification and variable modifications including methionine oxidation, protein N-terminal acetylation, deamidation of glutamine and asparagine as well as phosphorylation of serine, threonine and tyrosine (phosphoproteomics only). The peptide mass tolerance was 6 ppm and the MS/MS tolerance was 20 ppm. Database search was performed with Andromeda (Cox and Mann, 2008; Cox et al., 2011) against UniProt/Swiss-Prot human or mouse database (downloaded on 2014-11) with common serum contaminants and enzyme sequences. False discovery rate (FDR) was set to 1% at peptide spectrum match (PSM) level and at protein level. A minimum peptide count required for protein quantification was set to two. Normalized SILAC ratios were used for all analyses in this study except that non-normalized SILAC ratios were used for polysome proteome profiling to quantify relative abundance of individual proteins across density gradient fractions. Phosphorylation sites were ranked according to their phosphorylation localization probabilities (P) as class I ($P > 0.75$) (Olsen et al., 2006) and only class I sites were used for further analyses. Phosphorylation site occupancy was calculated based on the observed SILAC ratio for the phosphopeptide, the SILAC ratio for the non-phosphorylated peptide and the SILAC ratio of the protein (Olsen et al., 2010) using MaxQuant.

Data Analysis of PRM Measurements

Traces of all fragments from precursors in the spectral library (as exported from Picky) were extracted from all raw files using the Thermo MSFileReader software and the MSFileReader.py bindings written by François Allen. For each medium or heavy scan the normalized spectral contrast angle (SCN) was calculated (Toprak et al., 2014). Peaks were manually validated and required to have a SCN > 0.3 and >= 4 matched fragments in the medium or heavy channel. Further, peaks needed to be within a similar retention time range across all different measurements. From 50 proteins selected for PRM, 41 passed the quality filters and were thus included in the subsequent data-analysis. Ratios for each fragment using the maximum intensity

of each peak were calculated. All ratios were corrected by the median log2 fold ratio shift observed among all controls. The median log2 transformed ratio (log2FC) for each peptide in each raw-file was calculated from selected fragment ratios: The ten highest abundant fragments were selected from the peak with the highest detected SCN. Protein log2 FC were individually tested for differential significance against 0 using a one sided t-test ($p <= 0.05$). All peptide log2 FCs for a protein across all experiments (8 hr, 16 hr, label-swap experiments and two technical replicates) were therefore included in the test.

Estimation of Protein Abundance Using iBAQ

For each individual protein, intensity-based absolute quantification (iBAQ) algorithm (Schwanhäusser et al., 2011) computes the sum of all the peptides intensities divided by the number of theoretically observable peptides, which provides us rough estimation of protein abundance. To estimate protein abundance in the polysome fractions, iBAQ intensities of each protein was summed up from all polysome fractions and an average of summed iBAQ values from replicates was used for Figure 2H.

Generation of HEK293 Stable Cell Lines Expressing FLAG/HA-RPL12

RPL12 wild-type, S38A or S38D mutant coding sequences were recombined using LR Clonase II (Gateway, Thermo Fisher Scientific) into pFRT/TO/FLAG/HA-DEST (Addgene ID: 26360). The resulting vectors were used to generate stable HEK293 Flp-In T-Rex cells lines overexpressing FLAG/HA-tagged wild-type RPL12, or S38A and S38D RPL12 mutated proteins. Briefly, HEK293 Flp-In T-Rex cells were transfected in a 12-well format by mixing 100 µL of Opti-MEM with 1 µg of total plasmid DNA (9:1 ratio of pOG44 to destination vector) and 2 µL of Lipofectamine 2000 (Thermo Fisher Scientific). After a 5 min incubation, the transfection mixture was added to the cells. Cells were re-seeded into 10 cm dishes after 48 hr and allowed to attach overnight. Hygromycin (100 µg/mL, InvivoGen) was added the next day and the cells were selected for 2-3 weeks by the addition of fresh hygromycin-containing cell culture media every 2-3 days resulting in expansion of monoclonal colonies.

Generation of RPL12 Point Mutant Cell Lines via CRISPR/Cas9

RPL12-S38A and RPL12-S38D point mutant cells were generated by CRISPR/Cas9-mediated double strand break and homologous recombination. To generate pX330-Cas9-RPL12sgRNA plasmid, following synthetic oligos were annealed, phosphorylated and ligated into BbsI site of pX330-E2A-mCherry vector (Chu et al., 2015); RPL12sgS 5'-

CACCGCTACAGTCTCCGAAGAAAGT-3', RPL12sgAS 5'-AAACACTTTCTTCGGAGACTGTAGC-3'. For several known pseudo genes, specific targeting of RPL12 coding gene was confirmed by T7 assay using PCR primers of RPL12 seqfw 5'-TACTGCAGAGTTGTCTTAGTGAAGAAGG-3' and RPL12 T7rev 5'-GCTCCTTGAGGGCTTTGATGATCAGG-3' and lethality of homozygous mutants after electroporation into 19DN cells. To generate donor templates for knock-in, RPL12-S38A and RPL12-S38D PCR fragments were amplified from 19PP genomic DNA using following primers. For Rpl12-S38A donor template, BamHI-5HAfw 5'-CGGGATCCGTCTTTTCGGCTTTCGGCTCGGAGG-3', S38Arv 5'-CCAACTTTCTTCGGGGCCTGTAGAAATAATAGCATTCGTTACCATGTGCC-3', S38Afw 5'-GAATGCTATTATTTCTACAGGCCCCGAAGAAAGTTGGCGATGACATTGCC-3', EcoRI-3HArv 5'-CGGAATTCCAGAAAGTTCTCTAGCCAAAGACCGGTGTC-3'. For RPL12-S38D donor template, BamHI-5HAfw 5'-CGGGATCCGTCTTTTCGGCTTTCGGCTCGGAGG-3', S38Drv 5'-CCAACTTTCTTCGGGTCCTGTAGAAATAATAGCATTCGTTACCATGTGCC-3', S38Dfw 5'-GAATGCTATTATTTCTACAGGACCCGAAGAAAGTTGGCGATGACATTGCC-3', EcoRI-3HArv 5'-CGGAATTCCAGAAAGTTCTCTAGCCAAAGACCGGTGTC-3'. PCR fragments were digested by BamHI/EcoRI and ligated into BamHI/EcoRI sites of pBluescript II SK(+) vector for sequencing confirmation and to use as PCR template. To generate knock-in cell lines, pX330-Cas9-RPL12sgRNA plasmid and donor template were electroporated into 19DN cells by the Nucleofector 2b (Lonza) with X01 program. mCherry positive cells were FACS sorted on day 2 after the electroporation. After 3 days of mCherry positive cell culture, single cells were FACS sorted in 96 well plates. Genomic DNA was isolated from single cell clones using QuickExtract DNA Extraction Solution (Epicentre). Knock-in clones were identified by the PCR screening using KOD DNA polymerase (Merck Millipore) with following knock-in specific primers and external primer after the optimization of annealing temperatures. For RPL12-S38A screening, RPL12 exfw 5'- CGAGAGCTGAGCTTTTCCGCCTATATCC-3' and RPL12 A38rev 5'-ATGTCATCGCCAACTTTCTTCGGGGC-3'. For RPL12-S38D screening, RPL12 exfw 5'-CGAGAGCTGAGCTTTTCCGCCTATATCC-3' and RPL12 D38rev 5'-ATGTCATCGCCAACTTTCTTCGGGTC-3'. Homozygous knock-in clones were further selected by DNA sequencing to use in this study (Figure S5A). Cell sorting was done on a FACS Aria II (BD Biosciences). The mutations of the homozygous knock-in clones were further verified by LC-MS/MS; heavy-labeled parent cells were spiked into each knock-in clone, and knock-in specific peptides carrying RPL12 S38D or S38A mutation were quantified (see Figure S5B).

Western Blotting of Sucrose Density Gradient Fractions

HEK293 cells were lysed with the polysome buffer and the lysate was either treated with DMSO (control) or 10 mM EDTA. Following density gradient centrifugation, fractionation and protein precipitation were done as described above (see "Sucrose Density Gradient Centrifugation"). Each sample was re-suspended in 1 x LiDS loading sample buffer (Invitrogen) with 50 mM DTT and incubated at 70 ^{o}C for 5 min. The protein samples were loaded onto a 4%–12% gradient SDS-polyacrylamide gel (Thermo Fisher Scientific) and separated using electrophoresis. The proteins were then further transferred to a PVDF membrane (Merck Millipore) using a wet western blot contraption (Invitrogen) set to a constant current of 250 mA for 1 hr. The membranes were first blocked by incubating in 5% milk powder in Tris-buffered saline and 1% tween (TBS-tween) and then incubated with the protein specific antibody [anti-HA (sc-805 HA-probe Y-11, Santa Cruz), anti-RPL12 (PA5-31670, Thermo Fisher Scientific), anti-RPS5 (A304-011A, Bethyl Laboratories), anti-NUFIP2/82-FIP antibody (A301-600A-T, Bethyl Laboratories), anti-GPATCH4 antibody (A303-405A-T, Bethyl Laboratories), anti-LLPH antibody (SAB1302290), UQCRC2 antibody (GTX114873, GeneTex), H1FX antibody (ASB-OAAB10031, Aviva), anti-C11orf48 antibody (TA331749, Origene) and anti-C7orf50 antibody (20797-1-AP, Proteintech)] diluted 1:1,000 in 5% milk in TBS-tween overnight while rotating at 4 ^{o}C. Membranes were washed three times in TBS-tween and then incubated with secondary HRP-conjugated anti-rabbit or anti-mouse antibody (Sigma-Aldrich) diluted in 1:10,000 before being incubated with horseradish peroxidase (Merck Millipore).

AHA Labeling and Flow Cytometric Analysis

HEK293 and B cells were starved in methionine-free medium for 30 min and pulsed labeled with 1 mM azidohomoalanin (AHA) (Anaspec) for 30 min. Cells were then washed with ice-cold PBS and fixed in 4% PFA in PBS for 15 min at room temperature. Fixed cells were permeabilized with 1% BSA with 0.1% saponin in PBS for 15 min at room temperature and washed with 1% BSA in PBS. The click reaction was performed by incubating cells with 100 μL of the reaction mixture per sample [1 μM Alexa Fluor 488 alkyne (Thermo Fisher Scientific), 10 mM sodium ascorbic acid (Sigma-Aldrich) and 2 mM $CuSO_4$ (baseclick)] for 30 min in a dark room. After the click reaction, cells were washed once with 1% BSA. Then, cells were incubated with phospho-histone H3 Ser10 antibody (Cell Signaling Technology) and anti FLAG-biotin antibody (Miltenyi Biotec) (1:100 dilution, HEK293 only) for 1 hr at room temperature. After washing cells twice with 1% BSA, PE-Cy7 streptavidin secondary antibody (BioLegend) (1:400, HEK293 only) was added to samples and incubated for 30 min and then cells were washed twice with 1% BSA.

Cells were resuspended in FACS buffer (1% FCS, 1mM EDTA, 0.05% NaN3 in PBS). Flow cytometric analysis was performed on a FACS Aria instrument (BD Biosciences). FLAG/HA RPL12-expressing HEK293 cells were gated for measuring protein synthesis and cell cycle profile.

Pulsed SILAC (pSILAC)

HEK293 cells were seeded in SILAC "light" DMEM in a 6 well plate, and the following day cells were 40% confluent and transient transfections were performed using linear polyethylenimine (Sigma-Aldrich) with 2 µg plasmid DNA encoding RPL12-WT, -S38D or -S38A and 6 µg PEI per condition). After 72 hr post-transfection, cells were transferred to either SILAC "medium-heavy" or "heavy" media, respectively. After 24 hr pulse labeling, cells were harvested and combined, and proteins were digested to peptides as described above (see "Sample Preparation for Proteome Analysis"). For pSILAC and PRM assay using knock-in mouse B cells (60-70% confluent on the day of experiments), RPL12 S38D cells and RPL12 S38A cells were pulse labeled with either "medium-heavy" or "heavy" amino acids for 8 hr (both pSILAC and PRM assay) and 16 hr (PRM only). Label swap experiments were performed.

Immunoprecipitation of FLAG/HA-tagged RPL12 from Sucrose Gradient Fractions and Library Preparation

Cycloheximide (50 µg/mL) was added to each pooled 80S fraction (1 mL) obtained by sucrose gradient fractionation (Figure S4B). Aliquots of these input fractions were used for Western blot analysis (20 µL) and total RNA extraction with Trizol (50 µL). The rest of the sample was subjected to anti-FLAG immunoprecipitation. To prepare anti-FLAG conjugated magnetic beads, 15 µL of Dynabeads Protein G (Thermo Fisher Scientific) were used per sample, washed twice in 0.02 % of Tween 20/PBS (PBST) and resuspended in 30 µL of PBST containing 0.25 µg/µL anti-FLAG M2 monoclonal antibody (F3165, Sigma Aldrich). After a 1 hr incubation at room temperature with rotation, the beads were washed twice in PBST, resuspended into the fractionated sample, followed by incubation at 4 °C for 90 min. Next, the beads were concentrated and the supernatants removed, followed by 4 washing steps in 1 mL of washing buffer [0.05% (v/v) IGEPAL-CA630, 50 mM Tris pH 7.5, 150 mM KCl, 0.5 mM DTT, 50 µg/mL CHX, 1x complete EDTA-free protease inhibitor cocktail (Roche)]. Before concentrating the beads during the fourth washing step, 100 µL of suspension was removed for Western blot analysis, while the rest of the sample was used for RNA extraction. After the concentration of beads and removal of the supernatant, the beads were either resuspended in 1 bead volume of

2x Laemmli sample buffer (Western analysis) or 1 mL of Trizol (RNA extraction). After standard Trizol extraction consisting of chloroform addition and centrifugation, the clean-up of the aqueous phase was carried out using miRNAeasy kit (Qiagen) according to manufacturer's instruction.

Extracted RNA (either 1 µg of input samples or all of the immunoprecipitated material) was treated with 0.4 U Turbo DNase (Thermo Fisher) for 30 min at 37 ºC, phenol-chloroform extracted, ethanol-precipitated and resuspended in water.

For input samples, equal amounts of total RNA (1 µg) and 2 µL of 1:100 dilution of ERCC Spike-in Control Mix 1 (Thermo Fisher Scientific) were mixed and adjusted to 50 µL final volume with water. All immunoprecipitated material per sample was mixed with 2 µL of 1:100 dilution of ERCC Spike-in Control Mix 1 and adjusted to 50 µL final volume with water. These 50-µL samples were then input into the Truseq stranded mRNA kit (Illumina) using 2 rounds of oligo-dT enrichment. Manufacturer's instructions were followed in all subsequent steps. cDNA libraries from different samples were multiplexed using Illumina RPI oligonucleotides and sequenced by multiplexing 6 samples per lane on a HiSeq 2000 instrument using 1x101+7 cycles.

RNA-seq Data Processing and Analysis

Basecalls were converted to fastq files using Bcl2Fastq (v2.16.0.10). Next, the reads were demultiplexed and adapter sequences removed by Flexbar (v2.5) utilizing Illumina RPI index barcodes. Reads were then collapsed to remove PCR duplicates using collapse_reads.pl script (Jens, 2016; Lebedeva et al., 2011) and aligned to the human genome (version hg19) using the STAR aligner 2.4.2a with read counting mode enabled to obtain count tables. To account for the variability between input samples, we normalized the read counts by DESeq2-computed size factors (Love et al., 2014) obtained from ERCC spike-in read counts in the input samples. The same procedure was also applied to IP samples by using ERCC spike-in read counts from the IP samples. Next, pairwise comparisons of IP sample vs. input read counts were performed by DESeq2 using standard parameters. Log2-transformed fold changes provided in the DESeq2 output were used to quantify mRNA enrichment in IP vs. input.

To assess the effect of RPL12 mutations on translation during different cell cycle stages, we classified the immunoprecipitated mRNAs according to their enrichment values. Specifically, for

all positive log2-transformed enrichment values we calculated the difference in enrichment between three conditions (WT vs. S38A, WT vs. S38D or S38D vs. S38A). Next, we used R's quantile function to obtain three equally sized groups of mRNAs that showed high, unchanged and low enrichment in one condition. Distributions of changes in ribosome occupancy (mitosis vs. S phase) (Stumpf et al., 2013) for these three different groups of mRNAs were plotted (Fig. 5B) and Wilcoxon rank sum test to assess significant differences between them was used.

To assess sequence characteristics of precipitated mRNAs we first matched RNAseq data to coding sequences (release 91, from ensembl.org) based on ENSEMBL Gene ID. We considered one coding sequence per gene by removing duplicate entries. We then calculated frequencies for all 64 codons or the overall GC content and related them to the log2 D/A enrichment values across all matched genes. Spearman correlation coefficients of the individual pairwise comparisons are given and indicate the strength of the individual relationships.

For the comparison to transcriptional data we downloaded tables S5 (mitotically-expressed transcripts, here denoted as transcribed in mitosis) and S7 (mitotically-enriched transcripts, here denoted as transcriptionally induced in mitosis) from a dataset about mitotic transcription (Palozola et al., 2017). We matched transcripts to log2 D/A enrichment values from RNAseq data via ENSEMBL Gene IDs using db2db tool of bioDBnet (Mudunuri et al., 2009). Again, we considered one transcript per gene by removing duplicate entries. Further, we removed all entries in "transcriptionally enriched in mitosis" from "transcribed in mitosis". GC content of these gene sets was calculated as described above.

Ribosome Profiling for mouse B cells

The mouse B cells were cultured in two 15 cm plates per condition until 60-70 % confluent and incubated without treatments or with 100 ng/mL nocodazole (Sigma-Aldrich) for 8 hr to synchronize the cells in mitosis. Nocodazole was then released by washing the cells twice in pre-warmed PBS, and the cells were further incubated in fresh medium for 10 min before harvesting cells. Cellular DNA content was measured by flow cytometry (Figure S6G).

To verify expected changes in the abundance of mitotic marker proteins between asynchronous and nocodazole-treated cells, heavy-labeled asynchronous cells were spiked into the nocodazole-treated cells, and subsequent procedures including cell lysis, tryptic digestion and mass spectrometric analysis were described above (Figure S6H).

We followed the original protocol (Ingolia et al., 2012) with minor modifications (Calviello et al., 2015). Cell pellets were flash-frozen in liquid nitrogen, transferred to ice and lysed in mammalian polysome buffer [20 mM Tris-HCl, pH 7.4, 150 mM NaCl, 5 mM $MgCl_2$, 1 mM DTT, 100 µg/mL CHX), supplemented with 1% (v/v) Triton X-100 and 25 U/mL TurboDNase (Thermo Fisher Scientific)]. Afterwards, lysates were triturated ten times through a 26-gauge needle, cleared by centrifugation (20.000 *xg*, 5 min, 4 ^{o}C), flesh frozen in liquid nitrogen and stored at -80 ^{o}C. To obtain ribosome-protected fragments, lysates (120-µL aliquots) were treated with 3 µL of RNase I (Ambion, AM2294, 100 U/µL) for 45 min at room temperature with slow agitation. RNase activity was inhibited by the addition of 4 µL of SUPERaseIn (Thermo Fischer Scientific, AM2696, 20 U/µL). Meanwhile, MicroSpin S-400 HR columns (GE Healthcare, 27-5140-01) were equilibrated with 3 mL of mammalian polysome buffer without DTT and CHX by gravity flow and emptied by centrifugation at 600 x *g* for 4 min. We then immediately loaded 100 µL of the digested lysate on the column and eluted the column by centrifugation at 600 x *g* for 2 min. We extracted RNA from the flow-through (approximately 125 µL) using Trizol LS (Life Technologies, 10296-010) in combination with the RNA Clean & Concentrator kit (Zymo Research). We then depleted ribosomal RNA fragments using the RiboZero Kit (Illumina, MRZH11124) and separated the remaining RNA on a 17% denaturing urea-PAGE gel (National Diagnostics, EC-829). The size range from 27 nt to 30 nt, defined by loading with 20 pmol each of Marker-27 nt and Marker-30 nt, was cut out, and the RNA fragments were subjected to small RNA cloning and library generation (Hafner et al., 2012) using 3′ adaptor 4N-RA3, 5′ adaptor OR5-4N, RT primer RTP and PCR primers RP1 (forward primer) and RPI1-12 (reverse primer, containing barcodes, for sequences see Illumina Truseq small RNA oligonucleotides).
To obtain matching 3' mRNA-seq datasets for mRNA quantification, we isolated total RNA from mammalian polysome buffer lysates (120-µL aliquots, see above) using Trizol LS. Next, 1 µg of total RNA was mixed with 1 µL of 1:50 dilution of ERCC Spike-in Control Mix 1 (Thermo Fisher Scientific), TurboDNase-treated and input into QuantSeq 3' mRNA-Seq Library Prep Kit FWD (Lexogen, Inc.). Subsequent steps were performed according to manufacturer's instruction. All cDNA libraries were multiplexed at 12 samples per lane and sequenced on a HiSeq 2500 instrument using 1x51+7 cycles.

The following oligonucleotides were used for ribosome profiling:
Marker-27 nt, 5′-rArUrGrUrArCrArCrGrGrArGrUrCrGrArGrCrUrCrArArCrCrCrGrC-P;
Marker-30 nt,

5′-rArUrGrUrArCrArCrGrGrArGrUrCrGrArGrCrUrCrArArCrCrCrGrCrArArC-P;
4N-RA3, 5’-rApp-NNNNTGGAATTCTCGGGTGCCAAGG-InvdT;
OR5-4N, 5′-rGrUrUrCrArGrArGrUrUrCrUrArCrArGrUrCrCrGrArCrGrArUrCrNrNrNrN;

Ribosome Profiling Data Processing and Analysis

Basecalls were converted to fastq files using Bcl2Fastq (2.16.0.10). For the ribosome profiling dataset, reads were demultiplexed and adapter sequences removed by Flexbar (2.5). Reads were then collapsed to remove PCR duplicates, followed by removal of random nucleotides (four on both 5’ and 3’ end of the reads) using fastx_trimmer (FASTX Toolkit 0.0.14). Reads aligning to rRNA sequences were removed by Bowtie2 (2.3.2) and the remaining sequences were aligned to the mouse genome (mm10) using STAR aligner (2.5.3a). The STAR genome index was built using annotation obtained from GENCODE (M14). Next, reads of 29 or 30 nucleotides in length were retained and counted in coding sequence (CDS) exons (-t CDS) using HTSeq-count (0.9.1). Quality control of ribosome profiling data was performed using RiboTaper (Calviello et al., 2015) and riboWaltz (Lauria et al., 2017).

For the 3’ mRNA-seq dataset, reads were demultiplexed by Flexbar (2.5) and adapter sequences removed by cutadapt (1.12). Next, reads were aligned to the mm10 genome using the STAR aligner 2.5.3a with read counting mode enabled to directly obtain read count tables.

To detect differences in translational efficacy, as well as in mRNA abundance and both effects (transcription and translation) we used DESeq2 (1.18.1) with an interaction term model as described (Chothani et al., 2017). Briefly, RPF read counts were normalized using the DESeq2 estimateSizeFactors function by taking into account all read counts. For 3’ mRNA seq, ERCC spike-in read counts were used to obtain normalization factors using the same function. DESeq2 was run with default parameters. We considered genes with *P*-adjusted value <0.1 and log2-transformed fold change >0 to be differentially translated between parent mitotic vs parent asynchronous conditions. Log2-transformed fold changes for downstream comparisons were taken directly from the DESeq2 output.

Identifying ribosome-associated proteins using mean squared deviation (MSD)

To identify ribosome-associated proteins within 40S, 60S and polysome fractions we compared abundance profiles of individual proteins with corresponding consensus profiles by computing MSD values (Andersen et al., 2003; Foster et al., 2006). First, to define consensus profiles of 40S, 60S and polysomes we used the following fractions #2-14, #6-14 and #15-36 as 40S, 60S and polysome fractions, respectively (see Figure S2A). Non-normalized SILAC ratios were first

transformed into log_2 space and then average profiles of core RPs across corresponding fractions were used as 40S, 60S and polysome consensus profiles. We only considered protein profiles that were quantified at least in four and ten fractions for 40S/60S and polysome fractions, respectively. We then compared individual protein profiles with the corresponding consensus profiles of 40S, 60S or polysome using MSD values. MSD was calculated as follows: the squared deviation of the profile for individual proteins was divided by the number of data points (Andersen et al., 2003; Foster et al., 2006) (see Figure 2B). Observed distribution of MSD values in HEK293 was shown in Figure 2C. To discriminate true positive interactors from false positive based on MSD values, we used a statistical analysis using a simulated false discovery rate (FDR). To this end, we generated a shuffled dataset where the protein profiles (that is, SILAC ratios) were shuffled for each individual fraction among the proteins and MSD values were calculated for the shuffled dataset as well (see Figure 2C grey bars). The cut-off was chosen as the (lowest) MSD value from 100 independent shuffling operations (nominal FDR=0) of individual replicates (dash line in Figure 2C). We categorized two sets of proteins as potential polysome associated. For category one, a potential polysome associated protein was required to be above the threshold in both replicates from at least one cell line. For category two,a protein was required to be above the threshold in at least one replicate. The best MSD value from both replicates was considered the final MSD value in the respective cell line (see Figure 2C).

The performance of our polysome proteome profiling approach was assessed by receiver-operator-characteristics (ROC). To do this, we first defined a set of true positive (a reference set) and true negative polysome associated proteins (shuffled protein profiles (see above)). The reference set includes proteins that are known to be ribosome related based on GO terms, STRING protein interaction database (Szklarczyk et al., 2017) and RNAi data (Badertscher et al., 2015; Wild et al., 2010) (see Table S2 for a complete list of the reference). The false positive rate and true positive rate were plotted at different MSD thresholds once including and once excluding ribosomal proteins as true positives (Figure 2E) and the plot in Figure 2E is based on the data of replicate 1 in HEK293 cells. For interaction mapping at subunit level (related to Figures 2J and S2C) a threshold of 0.7 $-log_{10}$(MSD) was set to separate 40S/60S interacting proteins from background.

For calculating MSD values for phospho-sites we used their non-log ratios over the entire gradient and used the protein corresponding to the respective phosphopeptide as a reference

profile. We required the phosphopeptide to be quantified in at least one fraction, same as the respective phosphoprotein. The best MSD value from both replicates was considered the final phospho MSD for the respective cell line (see Figure 3B). Calculations were performed using in-house made R-scripts.

Protein Complex Enrichment Analysis

We compared the polysome associated proteins to "riboproteome" from a previous study (Reschke et al., 2013). For comparison to the data from Reschke et al., we matched IPI identifier to HGNC-approved symbols using the cross reference v.3.87. The depicted venn diagrams in Figures 2A and 2D are based on HGNC-approved symbols excluding ribosomal proteins.

For protein complex enrichment analyses, we used a CORUM (the comprehensive resource of mammalian protein complexes) (Ruepp et al., 2010) core set database as a reference (Jan/2017). We tested two foreground sets of proteins, the polysome associated proteins (see above) and all proteins quantified at least one polysome fraction in both biological duplicates. The significance of protein complex enrichment was assessed with a Fisher's Exact test using a Uniprot human protein database (Jan/2017) as background. An alpha of 0.01 was set for significance.

QUANTIFICATION AND STATISTICAL ANALYSIS

The type of statistical test (e.g., Wilcoxon rank-sum or Fisher's exact test) is annotated in the Figure legend and/or in the Methods and Resources segment specific to the analysis. In addition, statistical parameters such as the value of n, mean/median, SEM, SD and significance level are reported in the Figures and/or in the Figure Legends. Statistical analyses were performed using R as described in Methods and Resources for each individual analysis.

DATA AND SOFTWARE AVAILABILITY

Data Resources

Proteomic raw datasets have been deposited to the ProteomeXchange Consortium via the PRIDE partner repository with the dataset identifiers PXD009292 (Polysome (phospho)proteome profiling for HEK293 and HeLa), PXD009268 (Polysome proteome profiling for mESC), PXD009307 (pSILAC in HEK293), PXD009267 (Polysome proteome profiling for B

cells), PXD009276 (pSILAC in B cells) and PXD010029 (PRM in B cells).
RAW datasets for RNA-seq and ribosome profiling have been deposited under GEO: GSE112187.

Supplemental figure titles and legends

Figure S1. Polysome proteome profiling for mESCs and profiles for ribosomal protein-like proteins (related to Figure 1)

(A) Experimental setup for 3P in mESCs. Mouse ES cells were grown in a standard cell culture medium. NIH3T3 cells labeled with "heavy" SILAC amino acids served as a reference. The procedure is the same as described in Figure 1. (B) Abundance profiles for individual ribosomal proteins (40S and 60S proteins are shown in blue and red, respectively) across density gradient fractions. (C) Representative profiles for ribosomal protein-like proteins (RPL22L1/eL22L1, RPL26L1/uL24L1 and RPL7L1/uL30L1) in HEK293. See Figure S3 for the all profiles.

¶

Figure S2. Interaction mapping and validation (related to Figure 2)

(A) A schematic diagram showing density gradient fractions used for MSD calculation to map protein interaction with the 40S complex (fractions 2-14), 60S complex (fractions 6-14) and polysomes (fractions 15-36). (B) Correlation of polysome MSD values between HeLa duplicate samples (left) and between HEK293 and HeLa (right). Venn diagram representing the overlap of number of proteins identified in polysome fractions between two conditions is shown in the inset. (C) Mapping polysome interactome at subunit resolution in HeLa. (D) Validation for new polysome-associated proteins: Western blots for selected new candidates on sucrose gradient fractions in the absence (top) or presence (bottom) of EDTA. Western blots for RPs (RPS4/uS7 and PPL12/uL11) are shown as positive controls. (E) 3P-based profiles for the candidate proteins (dark green) are shown and insets show respective Western blots. NUFIP2 is used as a positive control.

¶

Figure S3. Western blot analysis using HEK293 stable cell lines expressing FLAG/HA-RPL12/uL11 (clone #2) (related to Figure 3) and RNA-seq analysis of monosome-associated mRNAs (related to Figure 5)

(A) Western blots of sucrose gradient fractions using an anti-HA antibody with short (top) and long (bottom) exposure time. The results for these different clones are consistent with the results shown in Figure 3E. (B) Experimental procedure. FLAG/HA RPL12/uL11 monosome-bound mRNAs were obtained by isolating monosomes from the corresponding density gradient fractions, followed by anti-FLAG immunoprecipitation (IP). (C) Immunoprecipitated mRNAs are classified according to their enrichment values (IP vs input). Specifically, for all positive log2 enrichment values we calculated the ratio between three conditions (WT vs. S38A, S38D vs. S38A or WT vs S38D). Next, we used a quantile function to obtain three equally sized groups of mRNAs with high, unchanged and low ratios for a given comparison. (D) Distributions of changes in ribosome occupancy (mitosis vs. S phase) (Stumpf et al., 2013) for the three different groups of mRNAs were plotted. P values were calculated using one sided Wilcoxon rank sum tests.

¶

Figure S4. Characterization of mouse B cells (related to Figure 6)

(A) Verifying RPL12 point mutation in mouse B cells: Sequencing results at the *rpl12* target. Defined point mutations and homozygous knock-in clones were verified and selected using knock-in specific primers (see STAR method for the oligonucleotides used in this study). (B) Mass spectrometric analysis for the knock-in cell lines. “Heavy” SILAC labeled-parent cells were spiked into each knock-in cell line grown in a normal medium. Representative MS spectra for the tryptic peptides carrying corresponding point mutations are shown. The knock-in specific RPL12 peptides carrying the point mutations (S38D: IGPLGLDPK or S38A: IGPLGLAPK) were exclusively observed in the corresponding knock-in cell lines while the RPL12 WT peptide (WT: IGPLGLSPK) was exclusively observed in the parent cells. Note that an RPL12 peptide (EILGTAQSVGCNVDGR) not overlapping with the mutation site was observed in all the cell lines. (C) Experimental setup for 3P in mouse B cells. The parent cells labeled with "heavy" SILAC amino acids were served as a reference. The procedure is the same as described in Figure 1. (D) Averaged abundance profiles for individual ribosomal proteins (40S and 60S proteins are shown in blue and red, respectively) across the density gradient. RPL12's profiles are shown in purple.

¶

Figure S5. pSILAC and ribosome profiling for mouse B cells (related to Figure 6)

(A) Cumulative distribution function (CDF) plots of log2-fold changes (H/M ratios) of protein synthesis from the label swapping pSILAC experiment. P-values were computed using one-sided Wilcoxon-rank sum test. (B) PRM based validation of observed fold changes between

S38A and S38D cells for 41 proteins selected from the pSILAC data. Green check marks indicate proteins that go into the right direction and are significant. Green check marks in parentheses indicate proteins that go into the right direction but are not significant. Red crosses indicate proteins that do not go into the right direction. P-values were computed using one-sided Wilcoxon-rank sum test. (C) Correlation heatmap of individual ribo-seq (top) and RNA-seq (bottom) read counts: high correlation is observed between the libraries. The numbers represent Pearson correlation coefficients. (D) The principal component analysis indicates that different cell lines and cell cycle stages can be clearly distinguishable based on the ribo-seq and RNA-seq datasets. (E) RiboTaper output. Meta analysis of the periodicity of read starts around start codons. Number of reads at individual positions are shown. Colours correspond to different ORFs (0: green, +1: red,+2: blue). X-axis shows distance in nucleotides from the start codon. (F) Boxplots comparing pSILAC (Figure S5A) and ribosome profiling (Figure 6D) for the subsets based on log2 fold-changes (S38D/S38A) of the pSILAC data. P-values were computed using one-sided Wilcoxon-rank sum tests. (G) Representative DNA content profiles of asynchronous (straight lines) and nocodazole-treated (dashed lines) cells. Parent, S38D and S38A cells are shown in red, blue and light green, respectively. (H) Mitotic marker proteins exhibited higher abundance in the nocodazole-treated parent cells than in the asynchronous parent cells. To verify expected changes in the abundance of mitotic proteins in the nocodazole-treated cells, heavy-labeled asynchronous cells were spiked into the cells synchronized in mitosis. The scatter plot shows log2 fold-changes of the protein abundance (heavy-labeled asynchronous cells vs nocodazole-treated cells) between biological duplicate. Examples of known mitotic marker proteins are indicated by red dots. As expected, mitosis related GO terms such as "cell division" and "cytokinesis" are overrepresented for the proteins that exhibited higher abundance (log2 FC < -0.5 in both replicates, red dash line in the figure) in the drug treated cells than in asynchronous cells. (I) GO enrichment analysis for 692 genes that are preferentially translated in mitosis compared to AS in wild-type B cells. Adjusted p-values by Benjamini–Hochberg are shown.

Supplemental dataset title and legend

Supplementary dataset. Profiles for all 145 identified polysome interactors (class I) and 40 additional class II proteins (related to Figure 2)

Every page shows four profiles for both replicates in HeLa and HEK293 cells. Blue and red lines show median profiles of 40S and 60S core RPs. Orange lines show the profile of the individual polysome interactor. If an individual protein is considered to be a polysome interactor in a given

experiment its identifier and MSD value is depicted. Histograms show the distribution of MSD values with the position of the respective protein indicated by an arrow (see Figure 2C). The scatter plots depicts MSD values separately for 40S and 60S fractions to assess subunit-specific binding (see also Figure 2J and S2C). Class I and II category include proteins which passed a MSD cut-off in both biological replicates and proteins which only passed a cut-off in one of the two replicates in either cell line, respectively.

¶

Supplemental table titles

Table S1: A list of proteins and their MSD (mean squared deviation) values; related to Figure 2¶
Table S2: A reference for known ribosome-related proteins; related to Figure 2G¶
Table S3: pSILAC data for HEK293; related to Figure 5A¶
Table S4: RNA-seq data for HEK293; related Figure 5B¶
Table S5: pSILAC data for mouse B cells; related to Figure 6B¶
Table S6: Ribosome profiling data for mouse B cells; related to Figure 6D¶

¶

SUPPLEMENTAL INFORMATION ¶

Supplemental Information includes five figures and six tables and can be found with this article online.¶

¶

Highlights

- High resolution polysome proteome profiling across ribosomal subcomplexes
- Core ribosome of monosomes and polysomes does not differ significantly
- 145 proteins associate with actively translating polysomes
- Phosphorylation of RPL12/uL11 regulates translation during mitosis.

eTOC blurb

Multiple regulatory layers shape gene expression. Imami et al. show that protein production in mitosis is regulated by phosphorylation of the ribosomal protein RPL12/uL11.

Fig. 1

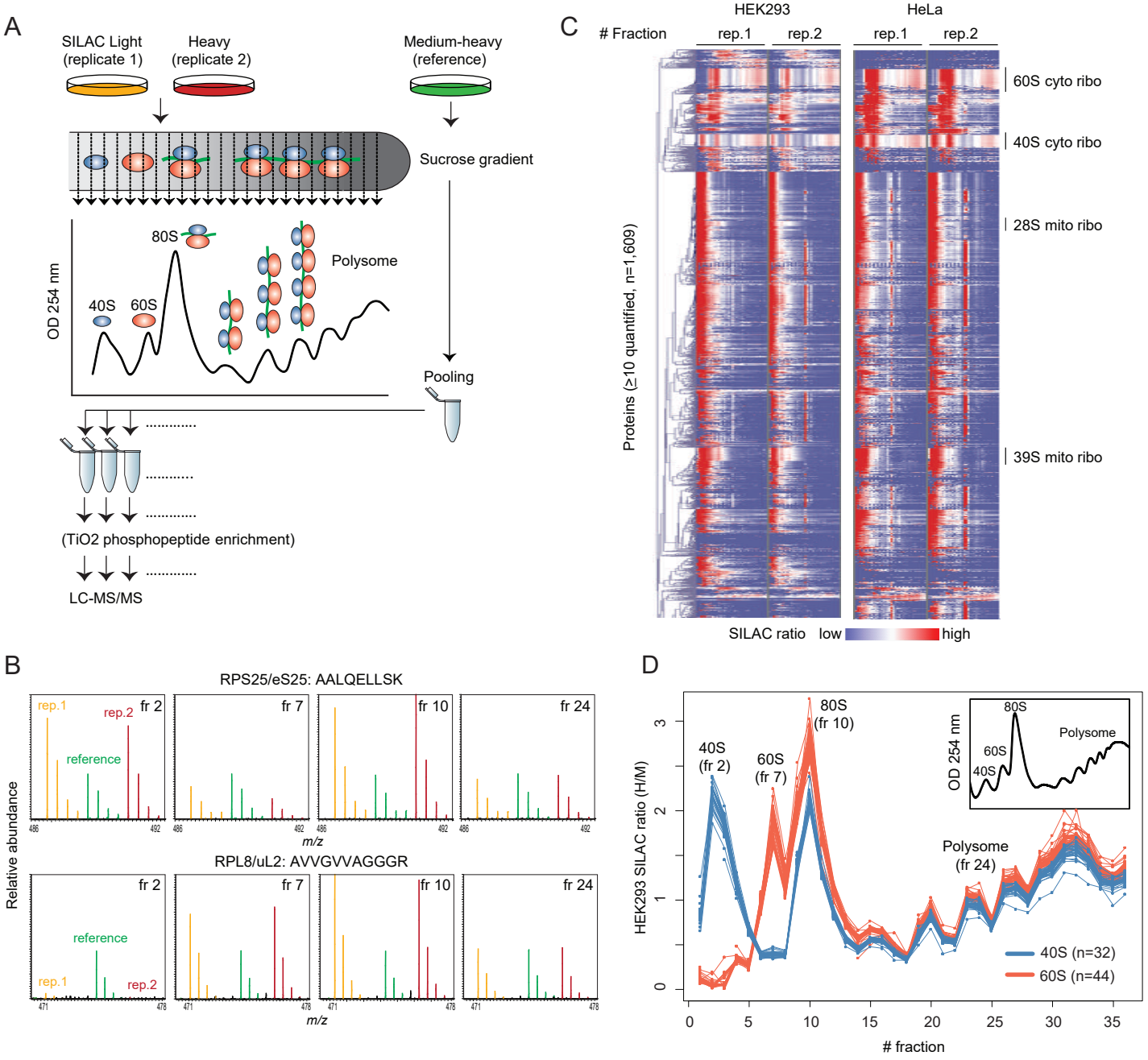
A
SILAC Light (replicate 1)
Heavy (replicate 2)
Medium-heavy (reference)
Sucrose gradient
80S
Polysome
40S
60S
OD 254 nm
Pooling
(TiO2 phosphopeptide enrichment)
LC-MS/MS
C
HEK293
HeLa
Fraction
rep.1
rep.2
rep.1
rep.2
60S cyto ribo
40S cyto ribo
28S mito ribo
39S mito ribo
Proteins (≥10 quantified, n=1,609)
SILAC ratio low high
B
RPS25/eS25: AALQELLSK
rep.1
rep.2
reference
fr 2
fr 7
fr 10
fr 24
Relative abundance
m/z
RPL8/uL2: AVVGVVAGGGR
D
HEK293 SILAC ratio (H/M)
40S (fr 2)
60S (fr 7)
80S (fr 10)
Polysome (fr 24)
OD 254 nm
40S (n=32)
60S (n=44)
fraction

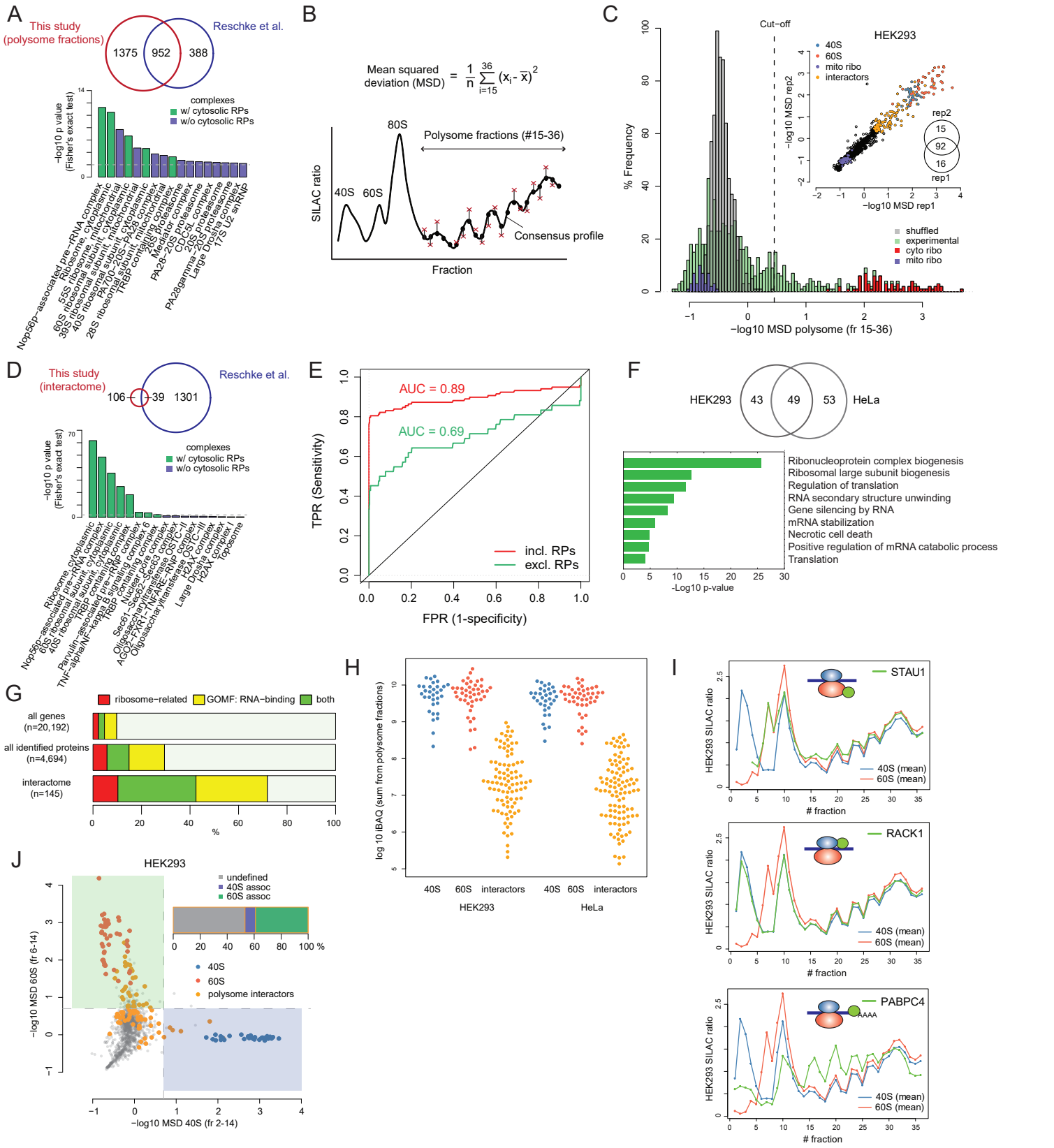
A
This study (polysome fractions)
Reschke et al.
1375
952
388
complexes
w/ cytosolic RPs
w/o cytosolic RPs
−log10 p value (Fisher's exact test)
Nop56p−associated pre−rRNA complex
Ribosome, cytoplasmic
55S ribosomal subunit, mitochondrial
39S ribosomal subunit, mitochondrial
40S ribosomal subunit, cytoplasmic
28S ribosomal subunit, mitochondrial
PA700−20S−PA28 complex
TRBP containing complex
Mediator complex
PA28−20S proteasome complex
CD5L proteasome
20S proteasome
PA28gamma 20S proteasome
Large Drosha complex
17S U2 snRNP
B
Mean squared deviation (MSD) = 1/n Σ (x_i − x̄)^2
80S
40S 60S
Polysome fractions (#15-36)
SILAC ratio
Consensus profile
Fraction
C
Cut−off
HEK293
40S
60S
mito ribo
interactors
−log10 MSD rep2
−log10 MSD rep1
rep2
15
92
16
rep1
% Frequency
shuffled
experimental
cyto ribo
mito ribo
−log10 MSD polysome (fr 15-36)
D
This study (interactome)
Reschke et al.
106
39
1301
complexes
w/ cytosolic RPs
w/o cytosolic RPs
−log10 p value (Fisher's exact test)
Ribosome, cytoplasmic
Nop56p−associated pre−rRNA complex
60S ribosomal subunit, cytoplasmic
40S ribosomal subunit, cytoplasmic
TRBP containing complex
Parylin−associated pre−RNA complex
TNF−alpha/NF−kappa B signaling complex
RBP containing complex 6
Nuclear−pore63 complex
Sec61−Sec62−Sec63 complex
AGO2−FXR1−NF−RE−RNP complex
Oligosaccharyltransferase OSTC−II
Oligosaccharyltransferase OSTC−I
H2AX complex III
Large Drosha complex I
H2AX complex I
Toposome
E
AUC = 0.89
AUC = 0.69
TPR (Sensitivity)
incl. RPs
excl. RPs
FPR (1-specificity)
F
HEK293
43
49
53
HeLa
Ribonucleoprotein complex biogenesis
Ribosomal large subunit biogenesis
Regulation of translation
RNA secondary structure unwinding
Gene silencing by RNA
mRNA stabilization
Necrotic cell death
Positive regulation of mRNA catabolic process
Translation
-Log10 p-value
G
ribosome−related
GOMF: RNA−binding
both
all genes (n=20,192)
all identified proteins (n=4,694)
interactome (n=145)
%
H
log 10 iBAQ (sum from polysome fractions)
40S
60S
interactors
HEK293
HeLa
I
STAU1
RACK1
PABPC4
HEK293 SILAC ratio
40S (mean)
60S (mean)
fraction
J
HEK293
undefined
40S assoc
60S assoc
40S
60S
polysome interactors
−log10 MSD 60S (fr 6-14)
−log10 MSD 40S (fr 2-14)

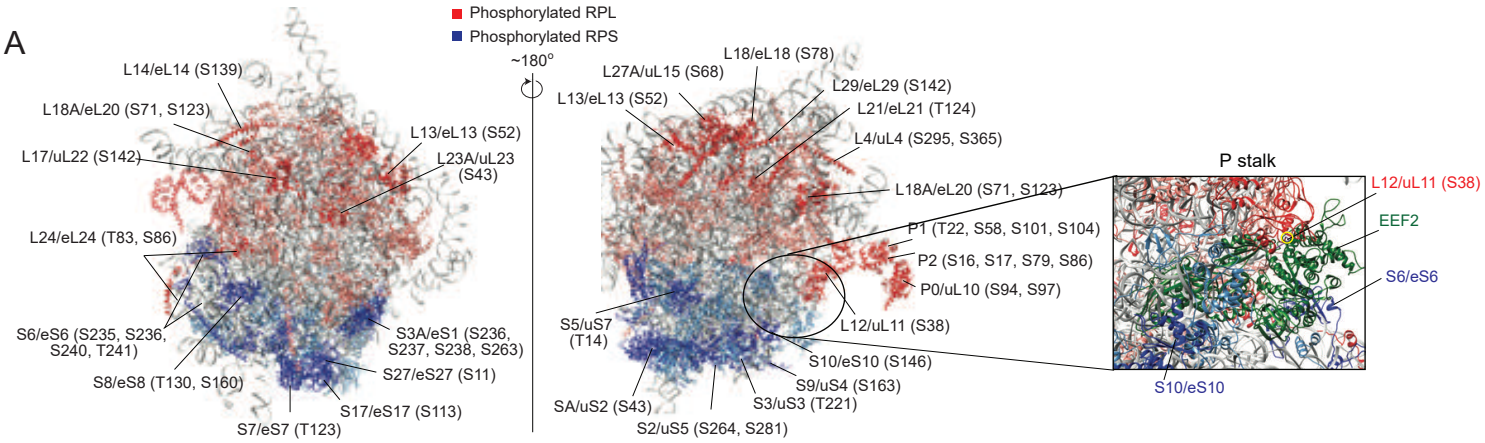
A
Phosphorylated RPL
Phosphorylated RPS
~180°
L14/eL14 (S139)
L18A/eL20 (S71, S123)
L13/eL13 (S52)
L17/uL22 (S142)
L23A/uL23 (S43)
L24/eL24 (T83, S86)
S6/eS6 (S235, S236, S240, T241)
S3A/eS1 (S236, S237, S238, S263)
S8/eS8 (T130, S160)
S27/eS27 (S11)
S17/eS17 (S113)
S7/eS7 (T123)
L18/eL18 (S78)
L27A/uL15 (S68)
L29/eL29 (S142)
L13/eL13 (S52)
L21/eL21 (T124)
L4/uL4 (S295, S365)
L18A/eL20 (S71, S123)
P1 (T22, S58, S101, S104)
P2 (S16, S17, S79, S86)
P0/uL10 (S94, S97)
S5/uS7 (T14)
L12/uL11 (S38)
S10/eS10 (S146)
S9/uS4 (S163)
SA/uS2 (S43)
S3/uS3 (T221)
S2/uS5 (S264, S281)
P stalk
L12/uL11 (S38)
EEF2
S6/eS6
S10/eS10

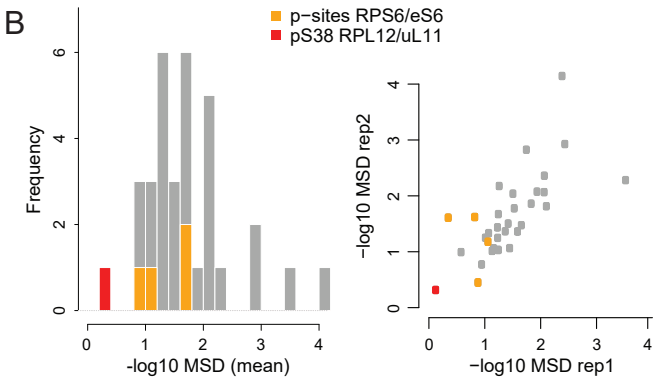
B
p−sites RPS6/eS6
pS38 RPL12/uL11
Frequency
-log10 MSD (mean)
−log10 MSD rep2
−log10 MSD rep1

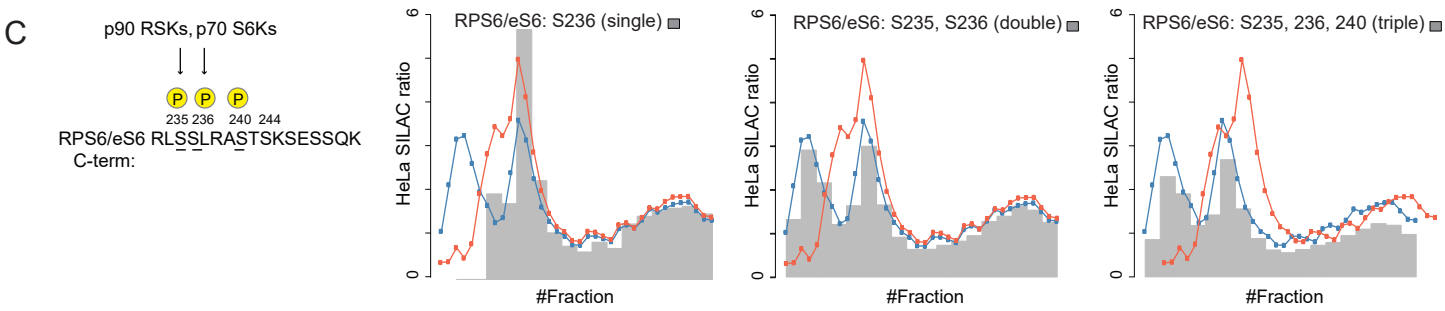
C
p90 RSKs, p70 S6Ks
P P P
235 236 240 244
RPS6/eS6 RLSSLRASTSKSESSQK
C-term:
RPS6/eS6: S236 (single)
RPS6/eS6: S235, S236 (double)
RPS6/eS6: S235, 236, 240 (triple)
HeLa SILAC ratio
#Fraction

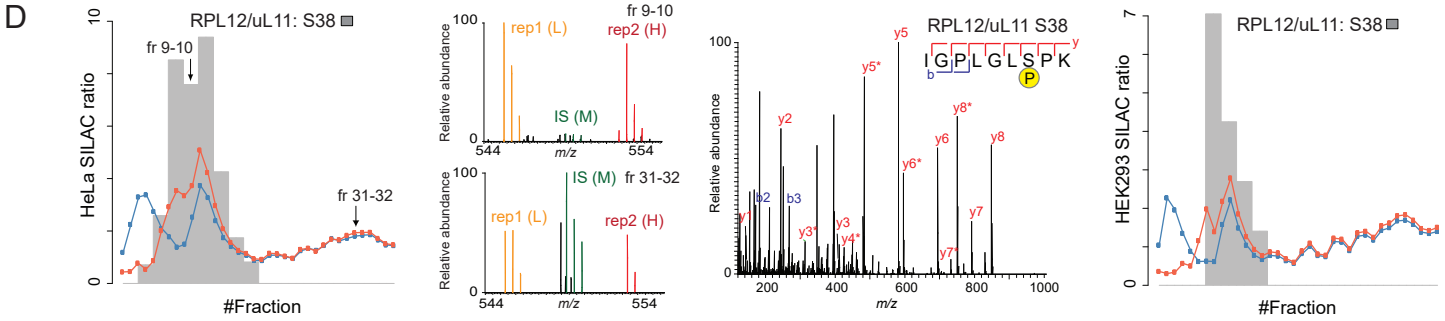
D
RPL12/uL11: S38
fr 9-10
fr 31-32
HeLa SILAC ratio
#Fraction
rep1 (L)
rep2 (H)
IS (M)
Relative abundance
m/z
RPL12/uL11 S38
I G P L G L S P K
P
HEK293 SILAC ratio

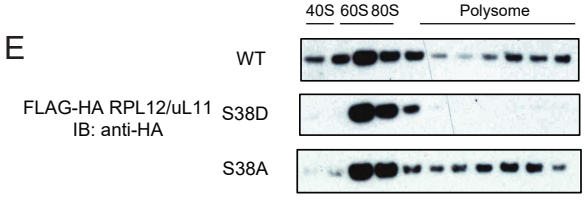
E
40S 60S 80S
Polysome
WT
FLAG-HA RPL12/uL11
IB: anti-HA
S38D
S38A

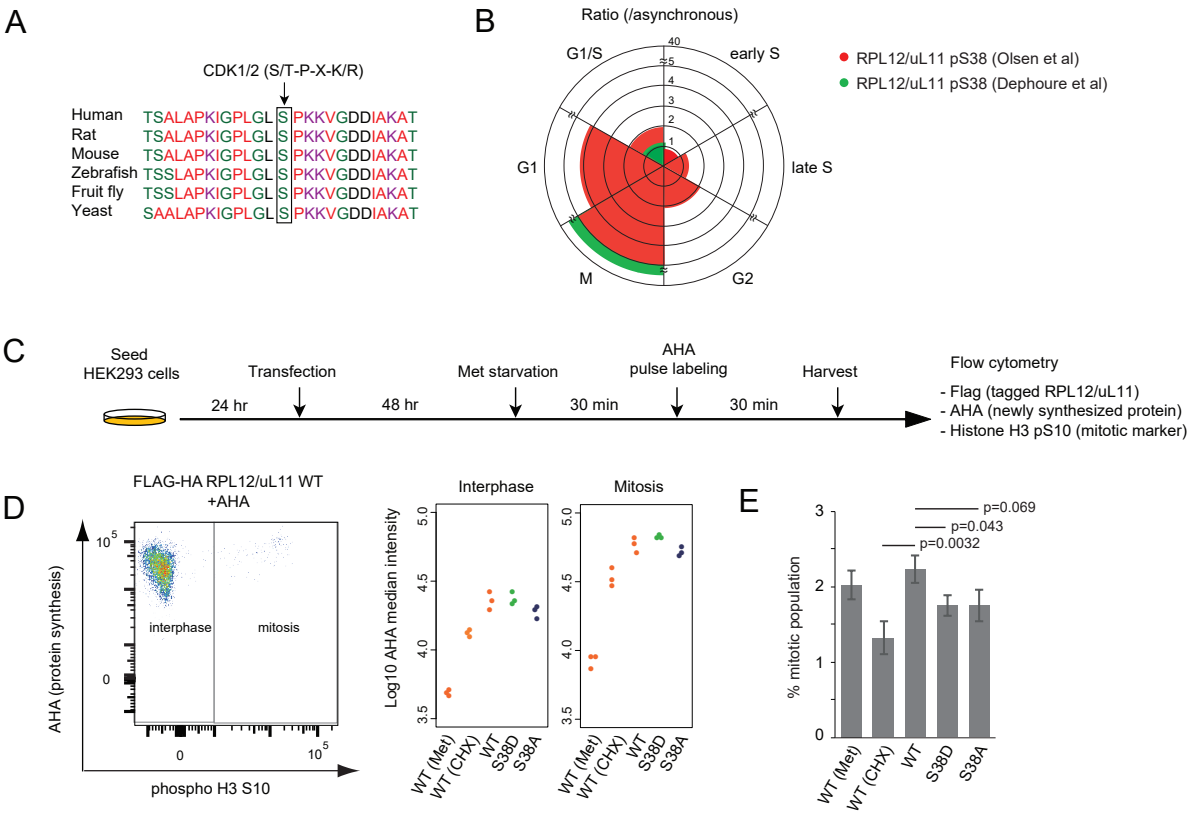
A
CDK1/2 (S/T-P-X-K/R)
Human TSALAPKIGPLGLSPKKVGDDIAKAT
Rat TSALAPKIGPLGLSPKKVGDDIAKAT
Mouse TSALAPKIGPLGLSPKKVGDDIAKAT
Zebrafish TSSLAPKIGPLGLSPKKVGDDIAKAT
Fruit fly TSSLAPKIGPLGLSPKKVGDDIAKAT
Yeast SAALAPKIGPLGLSPKKVGDDIAKAT
B
Ratio (/asynchronous)
G1/S
early S
late S
G2
M
G1
RPL12/uL11 pS38 (Olsen et al)
RPL12/uL11 pS38 (Dephoure et al)
C
Seed HEK293 cells
Transfection
24 hr
48 hr
Met starvation
30 min
AHA pulse labeling
30 min
Harvest
Flow cytometry
- Flag (tagged RPL12/uL11)
- AHA (newly synthesized protein)
- Histone H3 pS10 (mitotic marker)
D
FLAG-HA RPL12/uL11 WT +AHA
AHA (protein synthesis)
phospho H3 S10
interphase
mitosis
Interphase
Mitosis
Log10 AHA median intensity
WT (Mel)
WT (CHX)
WT
S38D
S38A
E
% mitotic population
p=0.069
p=0.043
p=0.0032

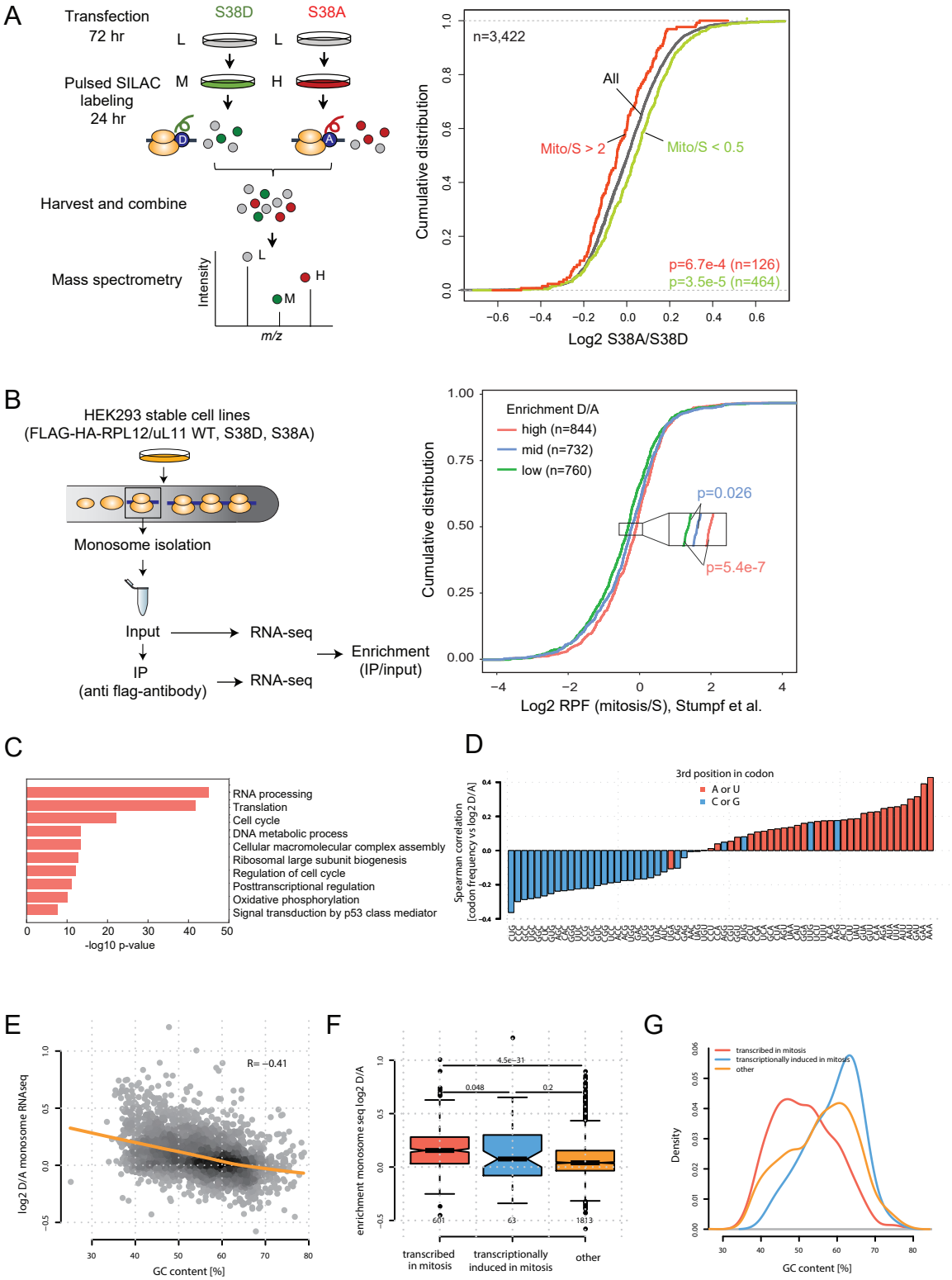
A
Transfection
72 hr
S38D
S38A
L
L
Pulsed SILAC
labeling
24 hr
M
H
Harvest and combine
Mass spectrometry
Intensity
m/z
n=3,422
All
Mito/S > 2
Mito/S < 0.5
p=6.7e-4 (n=126)
p=3.5e-5 (n=464)
Cumulative distribution
Log2 S38A/S38D
B
HEK293 stable cell lines
(FLAG-HA-RPL12/uL11 WT, S38D, S38A)
Monosome isolation
Input
RNA-seq
IP
(anti flag-antibody)
RNA-seq
Enrichment
(IP/input)
Enrichment D/A
high (n=844)
mid (n=732)
low (n=760)
p=0.026
p=5.4e-7
Cumulative distribution
Log2 RPF (mitosis/S), Stumpf et al.
C
RNA processing
Translation
Cell cycle
DNA metabolic process
Cellular macromolecular complex assembly
Ribosomal large subunit biogenesis
Regulation of cell cycle
Posttranscriptional regulation
Oxidative phosphorylation
Signal transduction by p53 class mediator
-log10 p-value
D
3rd position in codon
A or U
C or G
Spearman correlation
[codon frequency vs log2 D/A]
E
R= −0.41
log2 D/A monosome RNAseq
GC content [%]
F
4.5e−31
0.048
0.2
enrichment monosome seq log2 D/A
transcribed
in mitosis
transcriptionally
induced in mitosis
other
G
transcribed in mitosis
transcriptionally induced in mitosis
other
Density
GC content [%]

Fig. 6

B cell

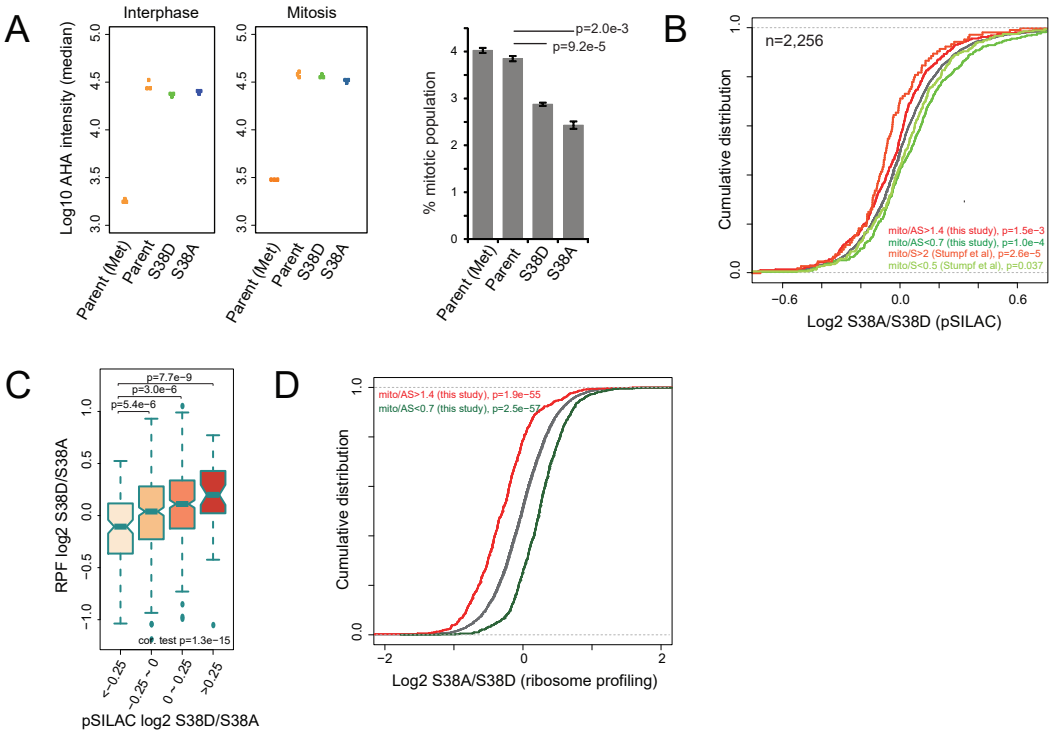
A
Interphase
Mitosis
Log10 AHA intensity (median)
Parent (Mel)
Parent
S38D
S38A
% mitotic population
p=2.0e-3
p=9.2e-5
B
n=2,256
Cumulative distribution
mito/AS>1.4 (this study), p=1.5e−3
mito/AS<0.7 (this study), p=1.0e−4
mito/S>2 (Stumpf et al), p=2.6e−5
mito/S<0.5 (Stumpf et al), p=0.037
Log2 S38A/S38D (pSILAC)
C
p=7.7e−9
p=3.0e−6
p=5.4e−6
RPF log2 S38D/S38A
cor. test p=1.3e−15
<−0.25
−0.25 ~ 0
0 ~ 0.25
>0.25
pSILAC log2 S38D/S38A
D
mito/AS>1.4 (this study), p=1.9e−55
mito/AS<0.7 (this study), p=2.5e−57
Cumulative distribution
Log2 S38A/S38D (ribosome profiling)

Fig. S1

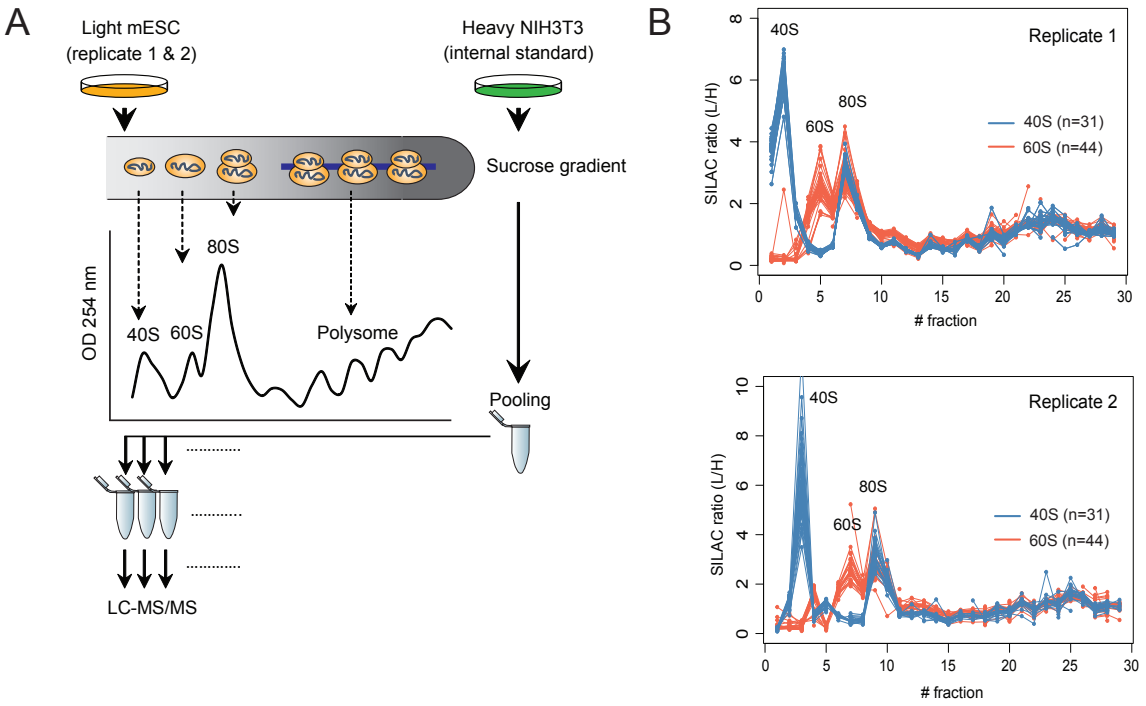
A
Light mESC
(replicate 1 & 2)
Heavy NIH3T3
(internal standard)
Sucrose gradient
80S
OD 254 nm
40S
60S
Polysome
Pooling
LC-MS/MS
B
Replicate 1
40S
60S
80S
40S (n=31)
60S (n=44)
SILAC ratio (L/H)
fraction
Replicate 2
40S
60S
80S
40S (n=31)
60S (n=44)
SILAC ratio (L/H)
fraction

Fig. S2

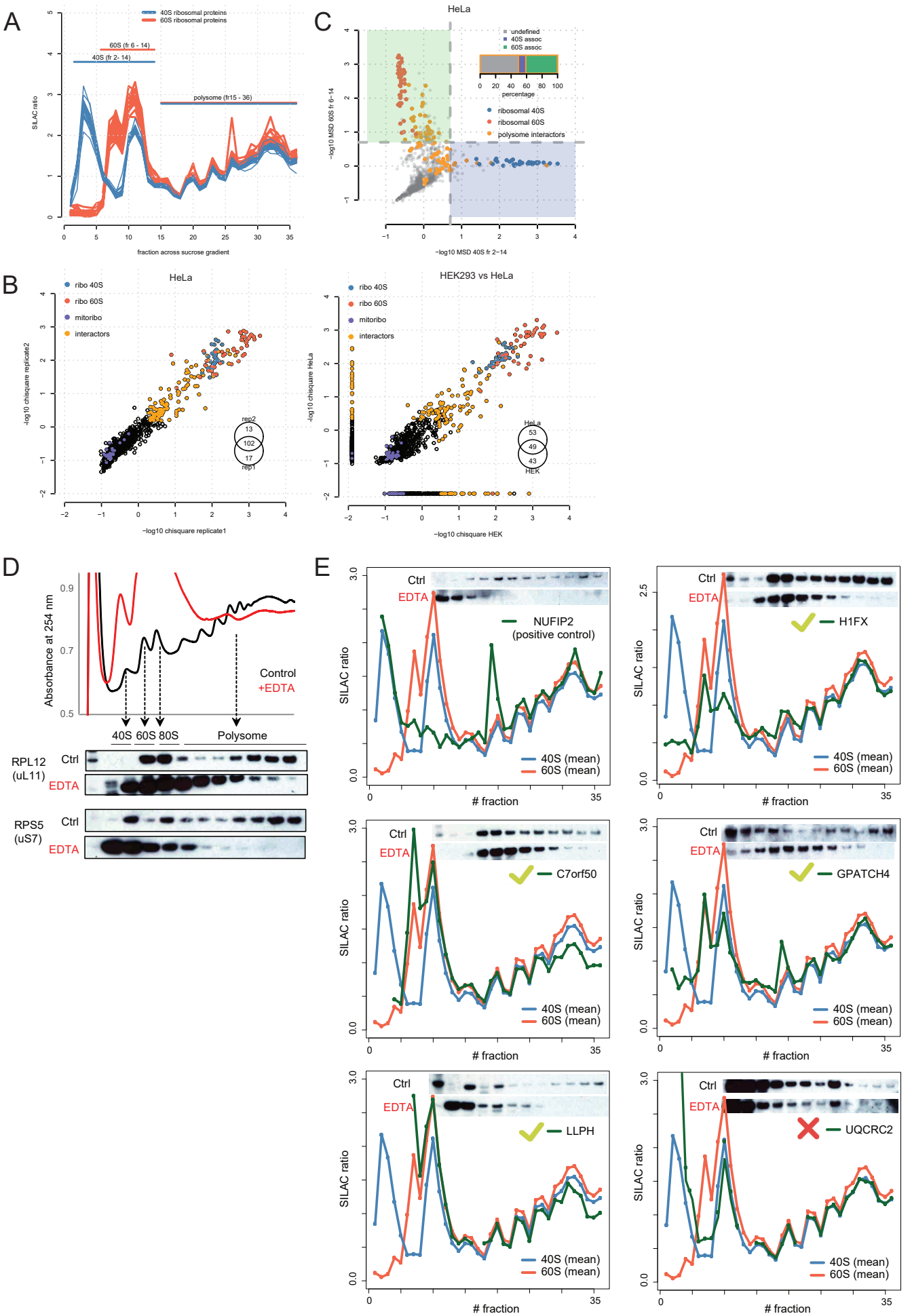
A
40S ribosomal proteins
60S ribosomal proteins
60S (fr 6 - 14)
40S (fr 2- 14)
polysome (fr15 - 36)
SILAC ratio
fraction across sucrose gradient
C
HeLa
undefined
40S assoc
60S assoc
percentage
ribosomal 40S
ribosomal 60S
polysome interactors
−log10 MSD 60S fr 6−14
−log10 MSD 40S fr 2−14
B
HeLa
ribo 40S
ribo 60S
mitoribo
interactors
−log10 chisquare replicate2
−log10 chisquare replicate1
rep2
rep1
HEK293 vs HeLa
−log10 chisquare HeLa
−log10 chisquare HEK
HeLa
HEK
D
Absorbance at 254 nm
Control
+EDTA
40S 60S 80S
Polysome
RPL12 (uL11)
RPS5 (uS7)
Ctrl
EDTA
E
NUFIP2 (positive control)
H1FX
C7orf50
GPATCH4
LLPH
UQCRC2
SILAC ratio
fraction
40S (mean)
60S (mean)

Fig. S3

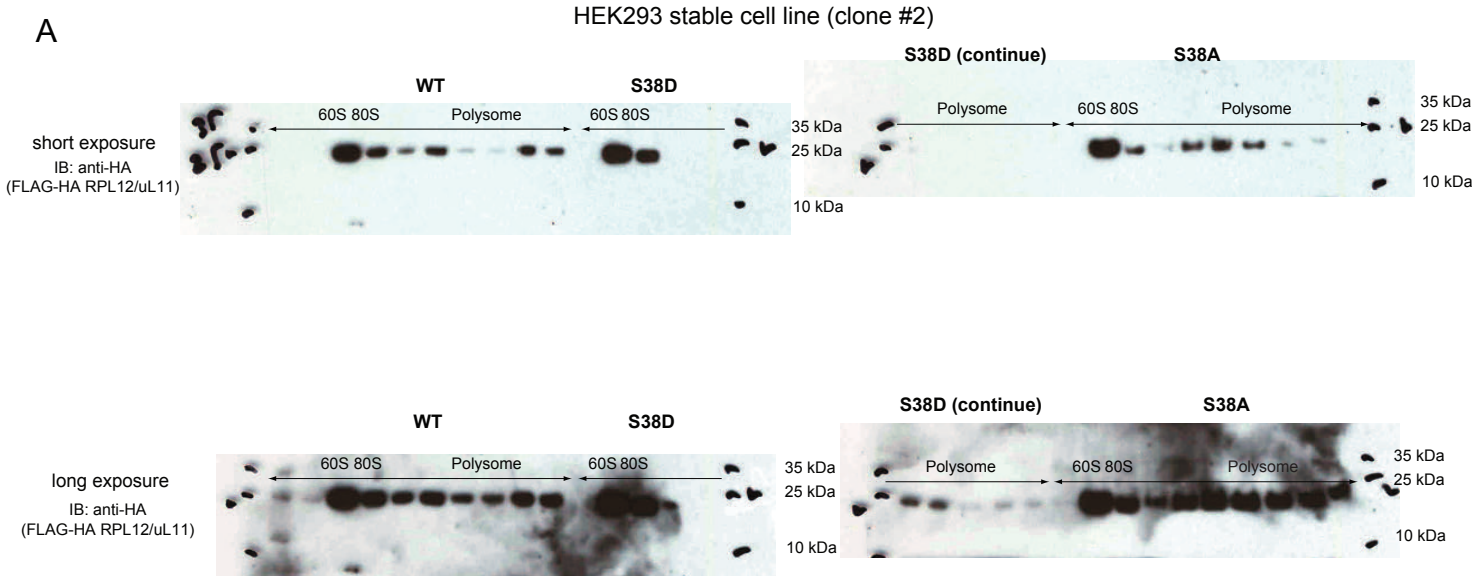
A
HEK293 stable cell line (clone #2)
WT
S38D
S38D (continue)
S38A
short exposure
IB: anti-HA
(FLAG-HA RPL12/uL11)
60S 80S
Polysome
35 kDa
25 kDa
10 kDa
long exposure
IB: anti-HA
(FLAG-HA RPL12/uL11)

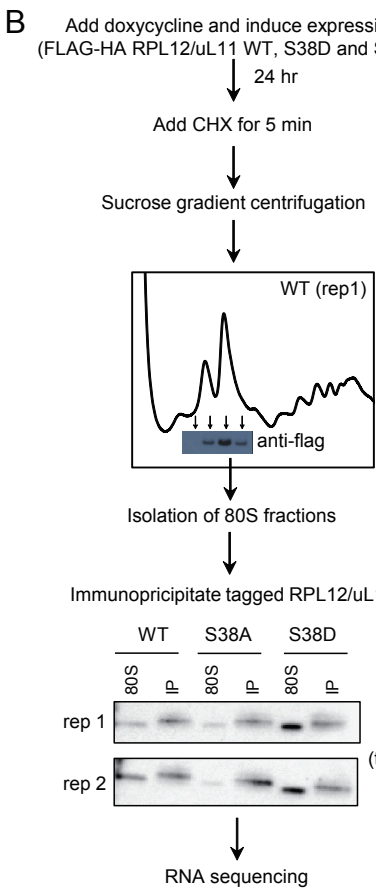
B
Add doxycycline and induce expression
(FLAG-HA RPL12/uL11 WT, S38D and S38A)
24 hr
Add CHX for 5 min
Sucrose gradient centrifugation
WT (rep1)
anti-flag
Isolation of 80S fractions
Immunopricipitate tagged RPL12/uL11
WT
S38A
S38D
80S
IP
rep 1
rep 2
anti-flag
(tagged RPL12/uL11)
RNA sequencing

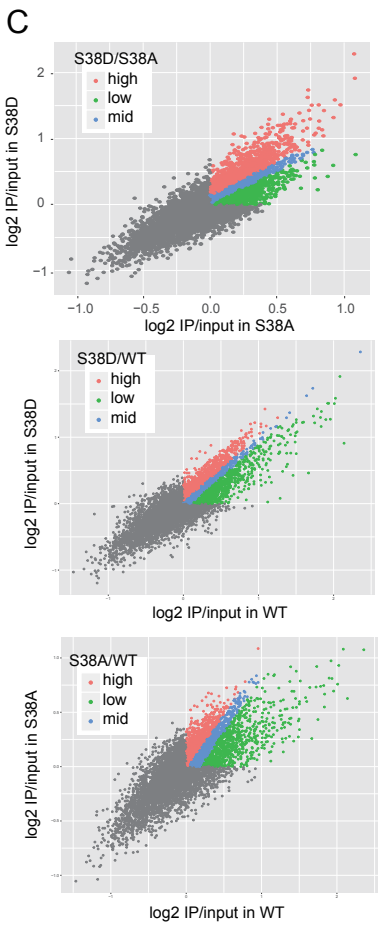
C
S38D/S38A
high
low
mid
log2 IP/input in S38D
log2 IP/input in S38A
S38D/WT
log2 IP/input in WT
S38A/WT

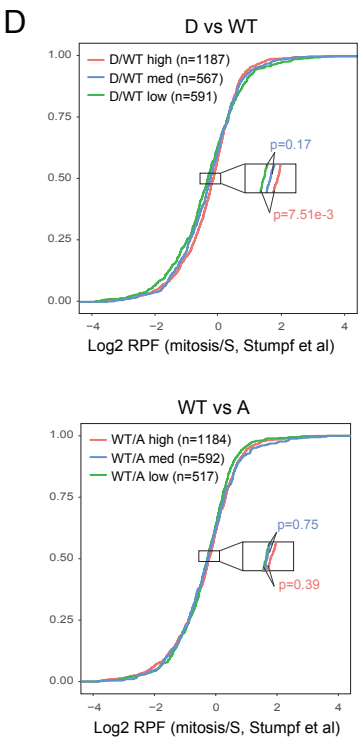
D
D vs WT
D/WT high (n=1187)
D/WT med (n=567)
D/WT low (n=591)
p=0.17
p=7.51e-3
Log2 RPF (mitosis/S, Stumpf et al)
WT vs A
WT/A high (n=1184)
WT/A med (n=592)
WT/A low (n=517)
p=0.75
p=0.39

Fig. S4

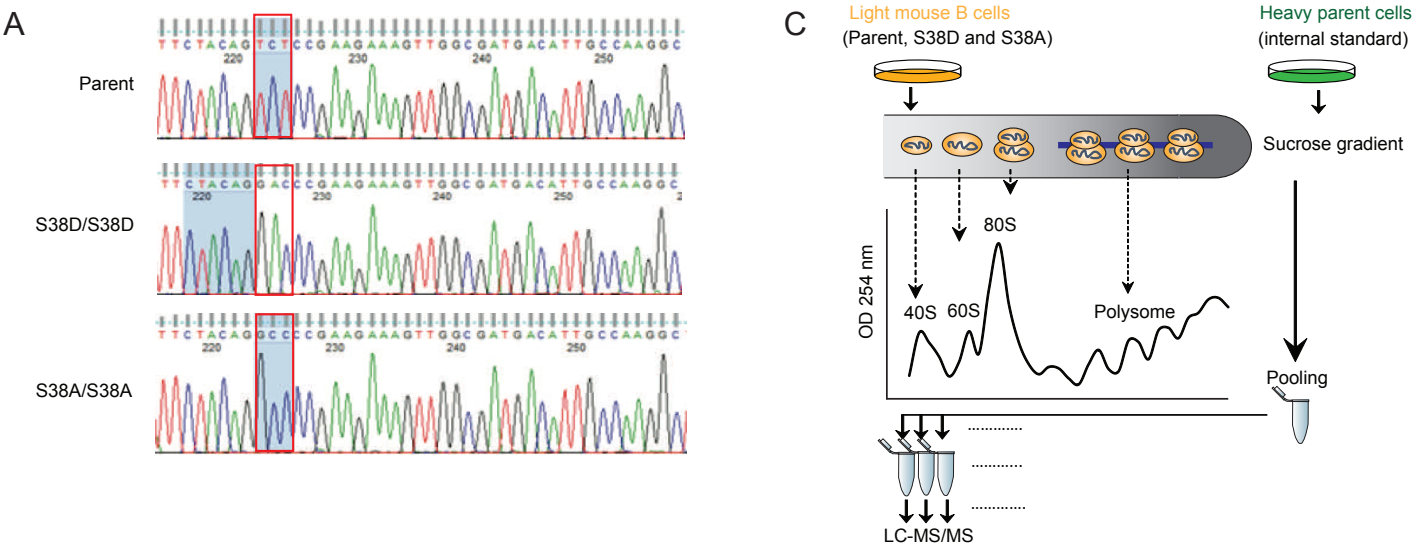
A
Parent
S38D/S38D
S38A/S38A
C
Light mouse B cells
(Parent, S38D and S38A)
Heavy parent cells
(internal standard)
Sucrose gradient
80S
OD 254 nm
40S
60S
Polysome
Pooling
LC-MS/MS

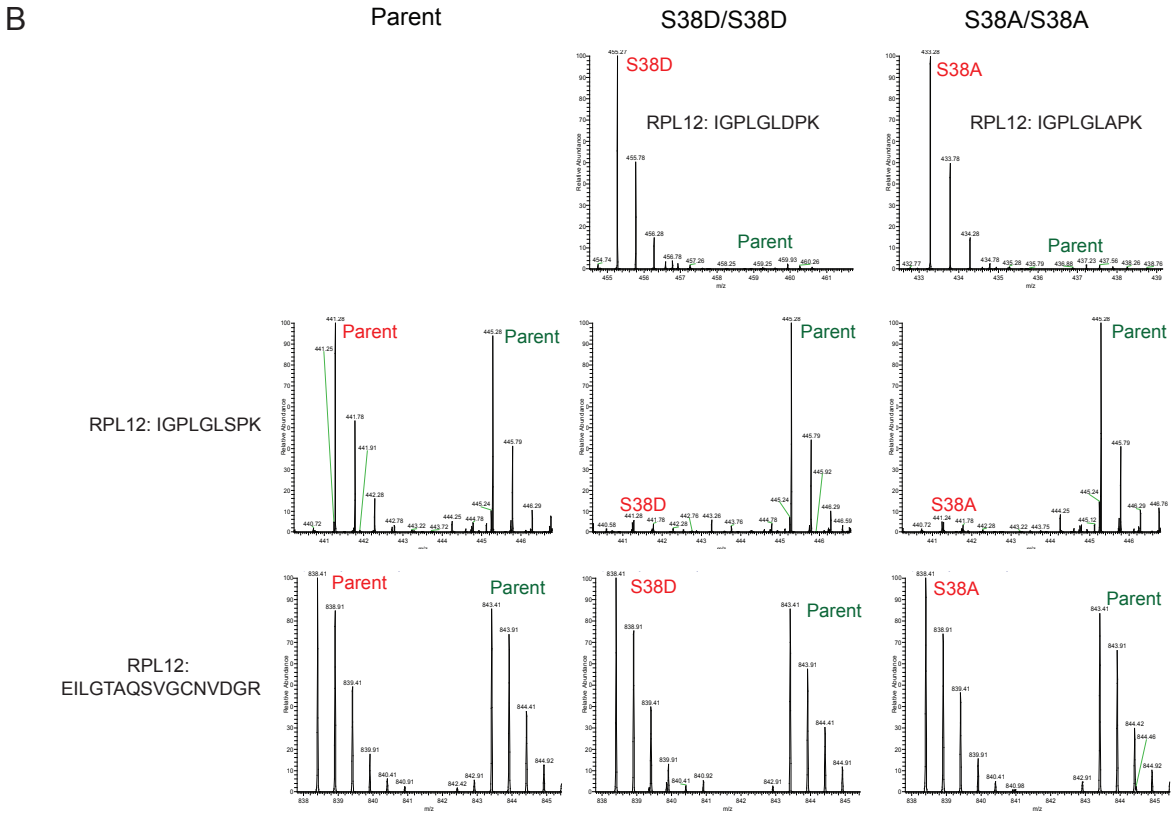
B
Parent
S38D/S38D
S38A/S38A
S38D
RPL12: IGPLGLDPK
S38A
RPL12: IGPLGLAPK
RPL12: IGPLGLSPK
RPL12:
EILGTAQSVGCNVDGR

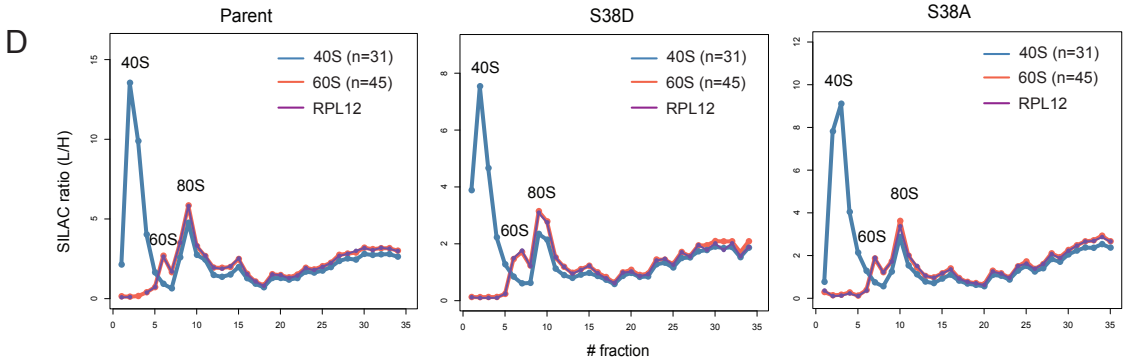
D
Parent
S38D
S38A
40S (n=31)
60S (n=45)
RPL12
40S
60S
80S
SILAC ratio (L/H)
fraction

Fig. S5

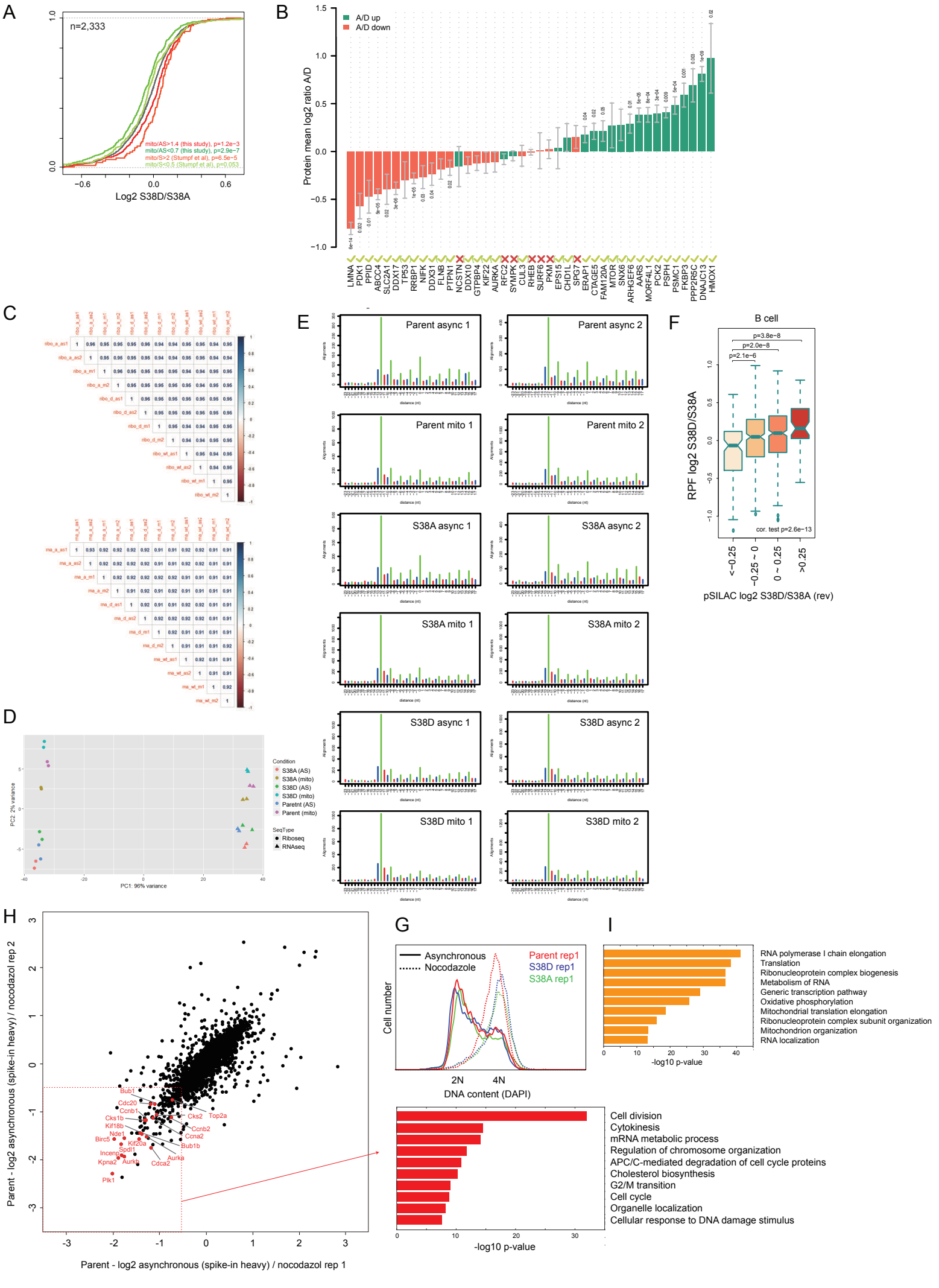
A
n=2,333
mito/AS>1.4 (this study), p=1.2e−3
mito/AS<0.7 (this study), p=2.9e−7
mito/S>2 (Stumpf et al), p=6.5e−5
mito/S<0.5 (Stumpf et al), p=0.053
Log2 S38D/S38A
B
A/D up
A/D down
Protein mean log2 ratio A/D
LMNA PDK1 PPID ABCC4 SLC2A1 DDX17 TP53 RRBP1 NIFK DDX31 FLNB PTPN1 NCSTN DDX10 GTPBP4 KIF22 AURKA RFC2 SYMPK CUL3 RHEB SURF6 PKM EPS15 CHD1L SPG7 ERAP1 CTAGE5 FAM120A MTOR SNX6 ARHGEF6 AARS MORF4L1 PCK2 PSPH PSMC1 FKBP3 PPP2R5C DNAJC13 HMOX1
C
D
PC2: 2% variance
PC1: 96% variance
Condition
S38A (AS)
S38A (mito)
S38D (AS)
S38D (mito)
Paretnt (AS)
Parent (mito)
SeqType
Riboseq
RNAseq
E
Parent async 1
Parent async 2
Parent mito 1
Parent mito 2
S38A async 1
S38A async 2
S38A mito 1
S38A mito 2
S38D async 1
S38D async 2
S38D mito 1
S38D mito 2
F
B cell
p=3.8e−8
p=2.0e−8
p=2.1e−6
cor. test p=2.6e−13
RPF log2 S38D/S38A
<−0.25
−0.25 ~ 0
0 ~ 0.25
>0.25
pSILAC log2 S38D/S38A (rev)
G
Asynchronous
Nocodazole
Parent rep1
S38D rep1
S38A rep1
Cell number
2N
4N
DNA content (DAPI)
H
Parent - log2 asynchronous (spike-in heavy) / nocodazol rep 2
Parent - log2 asynchronous (spike-in heavy) / nocodazol rep 1
Bub1
Cdc20
Ccnb1
Cks1b
Kif18b
Nde1
Birc5
Kif20b
Spdl1
Incenp
Kpna2
Aurkb
Plk1
Cdca2
Aurka
Bub1b
Ccna2
Ccnb2
Cks2
Top2a
-log10 p-value
Cell division
Cytokinesis
mRNA metabolic process
Regulation of chromosome organization
APC/C-mediated degradation of cell cycle proteins
Cholesterol biosynthesis
G2/M transition
Cell cycle
Organelle localization
Cellular response to DNA damage stimulus
I
-log10 p-value
RNA polymerase I chain elongation
Translation
Ribonucleoprotein complex biogenesis
Metabolism of RNA
Generic transcription pathway
Oxidative phosphorylation
Mitochondrial translation elongation
Ribonucleoprotein complex subunit organization
Mitochondrion organization
RNA localization